## ACKNOWLEDGEMENT

The author wishes to acknowledge the precious guidance and innumerable advices he received from Dr. W. Kozicki as well as the assistance of Drs. A. R. K. Rao and A. C. Tiu in conducting this project to term. He also wishes to thank G. Gasparetti and his assistants for the technical help they provided in constructing the apparatus.

Finally, I wish to thank my wife, Claire, for the patience and understanding she has shown during the course of this undertaking.

# TABLE OF CONTENTS

## LIST OF FIGURES

# LIST OF TABLES

## ABSTRACT

A theory, accounting for the anomalous behavior of certain high-molecular weight, dilute, polymer solutions flowing through closed channels is presented.

The flow is assumed to be steady, laminar and unidimensional, of the Poiseuille type.

The rheological characteristics of this type of non-Newtonian fluid were investigated using a capillary extrusion rheometer and polyethylene oxide solutions of very low concentrations. The system was operated over an intermediate shear stress range using three different tube diameters.

The line separations occuring on the flow diagrams are best explained by a polymer adsorption and desorption process taking place at the surface of the capillary wall, on a molecular basis. The associated drag reduction effect is also thought related to that sorption phenomenon.

The analysis also establishes the importance of the capillary tube diameter and of the applied shear stress in the theoretical and mathematical treatment of the results.

# I - INTRODUCTION

The primary aim of rheology is to formulate constitutive equations capable of describing the behavior of various fluids such as high-viscosity liquids, polymer melts, colloids, concentrated slurries, biological fluids, etc., which are of interest to the engineers.

Fluids are generally divided into two main categories; Newtonian and non-Newtonian. Newtonian fluids are characterized by a linear shear stress - shear rate relationship and comprise all gases and liquids, as well as solutions of low molecular weight compounds. Non-Newtonian fluids on the other hand, exhibit a non-linear flow curve, i. e., the viscosity of a non-Newtonian fluid is not constant at a given pressure and temperature but also depends on other factors such as the rate of shear of the fluid, the apparatus in which the fluid is contained or even the previous history of the fluid. Some examples of these fluids, which are of particular interest to the engineer are mentioned in the previous paragraph.

In the case of very dilute aqueous solutions of high molecular weight polymers, which we have been studying here, it is desirable that any proposed rheological model should represent the actual behavior of the fluid with reasonable accurracy.

Many models have already been proposed, including those of Savins[33] and more recently by Seyer and Metzner[37, 38], describing the flow from a viscoelastic point of view. These models are very complex mathematically and apply in transient flow situations. Since the flow we are directly dealing with is steady, laminar, one-dimensional, of the Poiseuille type, the time response of the fluid does not influence the flow.

Initially, five capillary tubes were used, to collect data over as wide a range as possible. However, a critical analysis of the results obtained indicated that the data from the two largest tubes was not reliable due to the fact that the length of the tubes to overcome the entrance length effect was not sufficient and this effect could not be evaluated without repeating the experiment using at least three different lengths of tubes for each diameter. Such experiments are now being conducted in a separate project which will hopefully attain the goals originally set for this investigation.

The study of laminar flow data was chosen, because it is now generally accepted that the drag reducing phenomenon occurring in turbulent flow, takes place in the laminar sublayer region near the wall[5, 36, 46]. Thus a clear understanding of the phenomenon occurring near the wall in laminar capillary flow should lead to useful deductions on the mechanism of drag reduction in turbulent flow.

At present[30], four types of drag reducing fluids are generally recognized, which are obtained by[1] the addition of small amounts of soluble polymers to the fluid[2], the addition of certain types of soap[3], the dilute suspension of properly sized particles and[4] the injection of a small annular film of viscoelastic fluid near the wall of a flowing system.

One of the main problems facing the engineer studying flow data for fluids exhibiting a surface effect is to find an efficient and simple method of evaluating those surface effects.

A method derived by Kozicki and coworkers[19], based on an extension of an analysis of the problem by Oldroyd[25], was used in our initial experiments. But it involved a lengthy trial and error procedure, without recourse to computational facilities, that did not make it attractive to engineers.

During the course of this work, a simpler, analytically accurate and direct method has been developed by Kozicki, which was subsequently used to evaluate and analyze for the effective velocity of slip at the wall, in the laminar flow of a drag reducing fluid.

## II - LITERATURE SURVEY

Drag reduction effects observed in the flow of a solution of polymethyl methacrylate in monochlorobenzene were first reported in the literature in 1949 by Toms[42]. In his honor, the phenomenon has received the name of "Toms' phenomenon".

Agoston et al.[1] were the first to report the same drag reducing effect in soap solutions, while working on the development of the flame thrower during World War II. In their case, they used napalm, an aluminum soap, dissolved in gasoline.

The Toms' phenomenon obtained while using dilute polymer solutions, has been repeatedly observed and reported in the literature by numerous workers including Savins[33], Shaver and Merril[39], Wells[45], Elata and Tirosh[9], Hoyt and Fabula[7], Goren and Norbury[13] and Ernst[10].

At the same time, four types of explanations are proposed currently in the literature[44] to elucidate the drag reduction phenomenon, namely:

1. "effective velocity of slip" at the wall, attributable directly to an increased laminar sub-layer thickness.
2. inherently delayed laminar to turbulent transition.
3. "anisotropic viscosity".
4. viscoelasticity.

Astarita[3], followed by Dodge and Metzner[8] inferred that the drag reduction occurs due to the suppression of turbulence and

of radial momentum transfer from large eddies in the vicinity of the wall. This explanation has been further developed by numerous authors[4, 23, 37, 38].

More recently, Hershey and Zakin[16] and Oliver and MacSporran[27] offered another explanation to the Toms' phenomenon which is based on the fact that the laminar to turbulent flow transition is extended beyond the usual zone. While this can be true for certain specific drag reducing fluids, it certainly does not constitute a basis for a generalized explanation of Toms' phenomenon.

The explanation appears to stem from the work of Kozicki[19] and Ernst[10, 11] who contend that the effective velocity of slip attributable to an increased laminar sub-layer thickness near the wall can well account for the observed pressure drop and friction factor reduction in the turbulent flow of dilute polymer solutions.

Kozicki and coworkers, working from velocity profile measurements made by Ernst succeeded in presenting a well documented case where two facts alone can explain the anomalous behavior of drag reducing fluids: a) polymer adsorption and/or alignment in the shear field in the region of the conduit wall, occurring in laminar flow, and b) a laminar sublayer thickness greater than that applicable to the purely viscous non-Newtonian fluids.

While it is true that viscoelasticity, as well as the drag reduction phenemenon are both functions of molecular properties inherent to the high molecular weight polymers used, one cannot conclude that the Toms' phenomenon is a manifestation of viscoelasticity although the above permits correlation with the viscoelasticity. This is especially true, in view of the fact that in the concentration ranges involved in the experiments, no noticeable viscoelasticity

has been observed even though drag reduction did occur[10, 11, 19] in turbulent flow.

One fact on which there now seems to be general agreement is the localization of the phenomenon in the vicinity of the wall. Wells and Spangler[46] found that an injection of a drag-reducing polymer solution in the vicinity of the wall in a flowing system produced the same effect as an homogeneous solution of the same type. Berman[5], using a different technique, found results pointing to an ordered molecular structure near the wall for a drag reducing polymer solution, while Seyer[36] studied theoretically, the effect of a small drag-reducing layer near a plate in a flowing system.

The effective slip velocity at the wall, as a convenient method of eliminating the diameter effect encountered in our experiment dates back to Schofield and Blair[34], who noticed this effect while experimenting with clay suspensions in water, although it should be pointed out that negative slip effects were not reported then. The technique was further developed by Mooney[25], Oldroyd[26], Jastrzebski[18] and Kozicki[20]. The method is further extended in this thesis and proves to be precise and simple in application.

## III - THEORETICAL FORMULATIONS

This section deals with the relationships developed in order to predict the effective slip velocity at the wall for fluids exhibiting anomalous wall effects in flow through closed circular conduits. The analysis is further carried on in order to evaluate the anomalous layer thickness and the non-Newtonian flow characteristics.

In the flow of certain non-Newtonian fluids, a separation phenomenon can be observed whereby, due to the velocity gradient near the tube wall, a thin layer of solvent is observed to form between the solid surface and the bulk solution[14]. The net effect of such a separation is similar to a reduction in viscosity in the vicinity of the wall and appears as actual slip between the solid surface and the bulk fluid.

But since actual slip is not believed to be happening, the phenomenon is referred to as an "effective slip velocity" near the wall.

On the other hand, the reverse phenomenon, whereby the more viscous material in solution adheres to the wall to form a polymer adsorption-gel, can also occur[32]. This results in a more viscous anomalous layer near the wall.

Therefore, whenever an anomalous effect occurs, it should be corrected accordingly in order to arrive at a correct shear stress - shear rate relationship.

a) Basic equations for non-Newtonian fluid flow, with wall effects, in a pipe.

For the steady, uniform, laminar and isothermal flow of fluids through circular pipes, Rabinowitsch[31] and Mooney[24]

developed an expression relating the average fluid velocity to the shear stress at the wall.

The derivation of the Rabinowitsch - Mooney equation, as modified by Kozicki, now follows:

The volumetric flow rate of a fluid in a pipe can be expressed as:

$$Q = \int\int U\,dA = 2\pi \int_0^R U r\,dr \quad \ldots\ldots\ldots\ldots \quad (1)$$

or

$$Q = \pi \int_0^R U\,d(r^2) \quad \ldots\ldots\ldots\ldots\ldots\ldots \quad (2)$$

if we now integrate Equation (2) by parts, we obtain:

$$Q = \pi \left[ U r^2 \Big|_0^R + \int_0^R r^2 \left( -\frac{dU}{dr} \right) dr \right] \quad \ldots\ldots\ldots \quad (3)$$

and since

$$U = U_w \quad \text{at} \quad r = R$$

where Uw is the effective velocity of slip at the wall of the tube; Equation (3) becomes

$$Q = \pi \left[ U_w R^2 + \int_0^R r^2 \left( -\frac{dU}{dr} \right) dr \right] \quad \ldots\ldots\ldots \quad (4)$$

From the momentum balance; we have

$$\frac{\tau}{\tau_w} = \frac{r}{R} \quad \ldots\ldots\ldots\ldots\ldots\ldots\ldots\ldots\ldots \quad (5)$$

Replacing Equation (5) into Equation (4), we obtain:

$$Q = \pi U_w R^2 + \frac{\pi R^3}{\tau_w^3} \int_0^{\tau_w} \tau^2 f(\tau)\,d\tau \quad \ldots\ldots \quad (6)$$

And from Equation (7), where

$$\langle U \rangle = Q/\pi R^2 \quad \ldots\ldots\ldots\ldots\ldots\ldots\ldots \quad (7)$$

Equation (6) becomes

$$\langle U \rangle = U_w + \frac{R}{\tau_w^3} \int_0^{\tau_w} \tau^2 f(\tau)\, d\tau \quad \ldots\ldots\ldots \quad (8)$$

And Equation (8) can be written as

$$\frac{8\left[\langle U \rangle - U_w\right]}{D} = \frac{4}{\tau_w^3} \int_0^{\tau_w} \tau^2 f(\tau)\, d\tau \quad \ldots\ldots \quad (9)$$

Then, to determine $f(\tau)$, we differentiate Equation (9), with respect to $\tau w$, using Leibnitz' rule:

$$\frac{d}{d\tau_w}\left[\frac{8(\langle U \rangle - U_w)}{D}\right] = -\frac{4 \times 3}{\tau_w^4} \int_0^{\tau_w} \tau^2 f(\tau)\, d\tau$$

$$+ \frac{4}{\tau_w^3} \cdot \tau_w^2 f(\tau_w) \quad \ldots\ldots\ldots\ldots \quad (10)$$

Replacing Equation (9) into Equation (10), we obtain

$$\frac{d}{d\tau_w}\left[\frac{8(\langle U \rangle - U_w)}{D}\right] = -\frac{3}{\tau_w}\left[\frac{8(\langle U \rangle - U_w)}{D}\right] + \frac{4}{\tau_w} f(\tau_w) \quad (11)$$

so that

$$f(\tau_w) = \frac{3}{4}\left[\frac{8(\langle U \rangle - U_w)}{D}\right] + \frac{\tau_w}{4} \frac{d}{d\tau_w}\left[\frac{8(\langle U \rangle - U_w)}{D}\right] \quad (12)$$

or, rearranging Equation (12), we can write;

$$f(\tau_w) = \frac{8(\langle U \rangle - U_w)}{D}\left[\frac{3}{4} + \frac{1}{4} \frac{d \ln\left[8(\langle U \rangle - U_w)/D\right]}{d \ln \tau_w}\right] \quad (13)$$

Here, $\frac{3}{4}$ and $\frac{1}{4}$ are geometric parameters applicable to flow in a circular tube only. In the most general case, they are replaced by b and a and Equation (13) then becomes the extended Rabinowitsch-Mooney equation postulated by Kozicki:

$$f(\tau_w) = \frac{8(\langle U\rangle - U_w)}{D}\left[b + a\,\frac{d\ln[8(\langle U\rangle - U_w)/D]}{d\ln\tau_w}\right] \qquad (14)$$

b) The flow behavior index.

The flow behavior index $\eta'$, for a circular capillary tube can be determined experimentally by using the relationship:

$$\eta' = \frac{d\ln\tau_w}{d\ln\left[\frac{8(\langle U\rangle - U_w)}{D}\right]} \qquad \ldots\ldots\ldots\ldots\ldots\ldots \qquad (15)$$

If Equation (15) is introduced into Equation (13), we obtain the following:

$$f(\tau_w) = \frac{3\eta' + 1}{4\eta'}\left[\frac{8(\langle U\rangle - U_w)}{D}\right] \qquad \ldots\ldots\ldots \qquad (16)$$

c) Effective velocity of slip.

The method used to evaluate the effective velocity of slip is analytically exact and stems from a mathematical manipulation of Equation (9) obtained in the development of the Rabinowitsch-Mooney equation.

Equation (9) is written as

$$\frac{8[\langle U\rangle - U_w]}{D} = \frac{4}{\tau_w^3}\int_0^{\tau_w}\tau^2 f(\tau)\,d\tau \qquad \ldots\ldots \qquad (17)$$

where the right-hand side is a function of $\tau_w$ only.

Therefore, Equation (17) can be rewritten as:

$$\frac{8\left[\langle U\rangle - U_w\right]}{D} = F(\tau_w) \quad \ldots\ldots\ldots\ldots\ldots\ldots \quad (18)$$

or

$$\frac{8\langle U\rangle}{D} = \frac{8U_w}{D} + F(\tau_w) \quad \ldots\ldots\ldots\ldots\ldots\ldots \quad (19)$$

Now, taking the partial derivative of Equation (19) with respect to $1/D$, at $\tau_w$ constant, we obtain:

$$\frac{\partial\left[8\langle U\rangle/D\right]}{\partial\left[1/D\right]}\Bigg|_{\tau_w} = \frac{\partial\left[8U_w/D\right]}{\partial\left[1/D\right]}\Bigg|_{\tau_w} + 0 \ldots\ldots \quad (20)$$

or, rearranging Equation (20),

$$\frac{8U_w}{D} = \int_0^{1/D} \left[\frac{\partial\left(8\langle U\rangle/D\right)}{\partial\left(1/D\right)}\right]_{\tau_w} d(1/D) \ldots\ldots \quad (21)$$

from which we obtain $U_w$, the effective velocity of slip.

From a graph of $\tau_w$ vs. $\langle U\rangle/D$, where different flow curves appear for each capillary tube diameter used, we can construct graphs of $8\langle U\rangle/D$ vs. $1/D$ at different values of $\tau_w$ as parameter.

Once these graphs are constructed, the slope of the lines at different $1/D$ values are read off the curves and plotted on another graph, versus $1/D$ again. This last graph is a representation of Equation (21), while the former represents Equation (20).

By calculating the area under the curves, on the $\partial\left(8\langle U\rangle/D\right)/\partial\left(1/D\right)$ vs. $1/D$ graphs, at the appropriate $1/D$ values, we therefore obtain the values of $8U_w/D$.

These values are then substracted from the original 8 $\langle U \rangle / D$ values in order to obtain a single flow curve corrected for the effective velocity of slip and the diameter effect.

d) Anomalous layer thickness.

From Oldroyd's analysis[26], the velocity gradient of the anomalous layer within a normal distance $\delta$, from the solid boundary can be represented as:

$$\frac{dU}{dy} = f(\tau) + g(\delta, \tau) \quad \ldots\ldots\ldots\ldots\ldots\ldots\ldots \quad (22)$$

where $f(\tau)$ is the velocity gradient characteristically ascribable to the fluid under laminar flow conditions and $g(\tau, \delta)$ is the correction term accounting for the anomalous behavior in the vicinity of the solid wall.

Outside of the anomalous layer, i.e., at $y > \delta$, the function $g(\tau, \delta) = 0$. Thus, the velocity $\langle U \rangle$ is given, in that region, by:

$$U = \int_0^y \left(\frac{dU}{dy}\right) dy \quad \ldots\ldots\ldots\ldots\ldots\ldots\ldots \quad (23)$$

and from Equation (22) and (23),

$$U = \int_0^{y>\delta} f(\tau)\, dy + \int_0^{\delta} g(\tau, \delta)\, dy \quad \ldots\ldots\ldots \quad (24)$$

If we designate

$$\int_0^{\delta} g(\tau, \delta)\, dy = U_w \quad \ldots\ldots\ldots\ldots\ldots\ldots\ldots \quad (25)$$

where Uw is the effective velocity of slip at the wall, then in general;

$$U = U_w + \int_0^{y>\delta} f(\tau)\, dy \quad \ldots\ldots\ldots\ldots\ldots\ldots \quad (26)$$

Two possible cases of anomalous behavior are represented in Figs. 1a and 1b.

(i) For separation

A thin layer of pure solvent, (water in our case) forms at the solid boundary, to which we can apply Newton's law of flow, so that;

$$\left(\frac{dU}{dy}\right) = \frac{\tau}{\mu_s} \quad \ldots\ldots\ldots\ldots\ldots\ldots\ldots\ldots \quad (27)$$

Replacing Equation (27) into Equation (22), we obtain;

$$\frac{\tau}{\mu_s} = f(\tau) + g(\tau, \delta) \quad \ldots\ldots\ldots\ldots\ldots\ldots \quad (28)$$

or

$$g(\tau, \delta) = \frac{\tau}{\mu_s} - f(\tau) \quad \ldots\ldots\ldots\ldots\ldots\ldots \quad (29)$$

and replacing Equation (29) into Equation (25) we have;

$$U_w = \int_0^{\delta} \left[\frac{\tau}{\mu_s} - f(\tau)\right] dy \quad \ldots\ldots\ldots\ldots\ldots \quad (30)$$

or

$$U_w \doteq \left[\frac{\tau_w}{\mu_s} - f(\tau_w)\right] \delta \quad \ldots\ldots\ldots\ldots\ldots\ldots \quad (31)$$

(ii) For adsorption

If we assume that $\left(\frac{dU}{dy}\right) = 0$ inside the distance $\delta$ from the wall, then Equation (22) becomes:

$$g(\tau, \delta) = - f(\tau) \quad \ldots\ldots\ldots\ldots\ldots\ldots\ldots \quad (32)$$

and replacing Equation (32) into Equation (25), we obtain:

$$U_w = - f(\tau_w)\, \delta \quad \ldots\ldots\ldots\ldots\ldots\ldots\ldots\ldots \quad (33)$$

Therefore, in the case of negative effective velocity of slip or adsorption of a polymer gel on the wall of the conduit, the anomalous layer thickness is represented by:

$$\delta = - U_w / f(\tau_w) \quad \ldots\ldots\ldots\ldots\ldots\ldots\ldots\ldots \quad (34)$$

while for positive effective velocity of slip or separation, the anomalous layer thickness is given by:

$$\delta = \frac{U_w}{\left[\frac{\tau_w}{\mu_s} - f(\tau_w)\right]} \quad \ldots\ldots\ldots\ldots\ldots\ldots\ldots\ldots \quad (35)$$

In both cases, $f(\tau_w)$ is given by:

$$f(\tau_w) = \frac{1 + 3\eta'}{4\eta'} \left[\frac{8(\langle U \rangle - U_w)}{D}\right] \quad \ldots\ldots\ldots \quad (36)$$

where $\eta'$ is the non-Newtonian flow behavior index calculated previously in section (b).

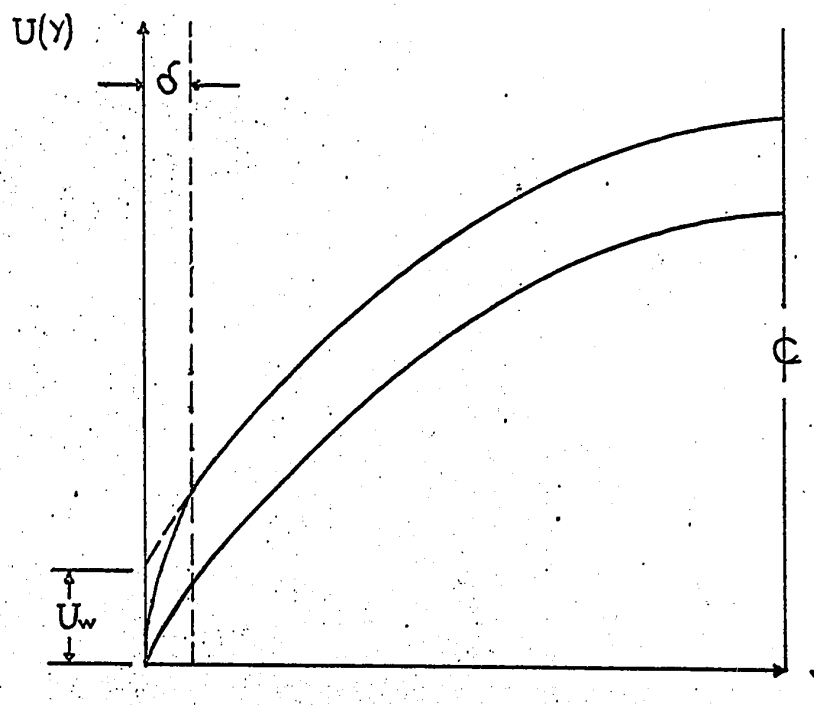


a) Positive Effective Velocity of Slip (Desorption)

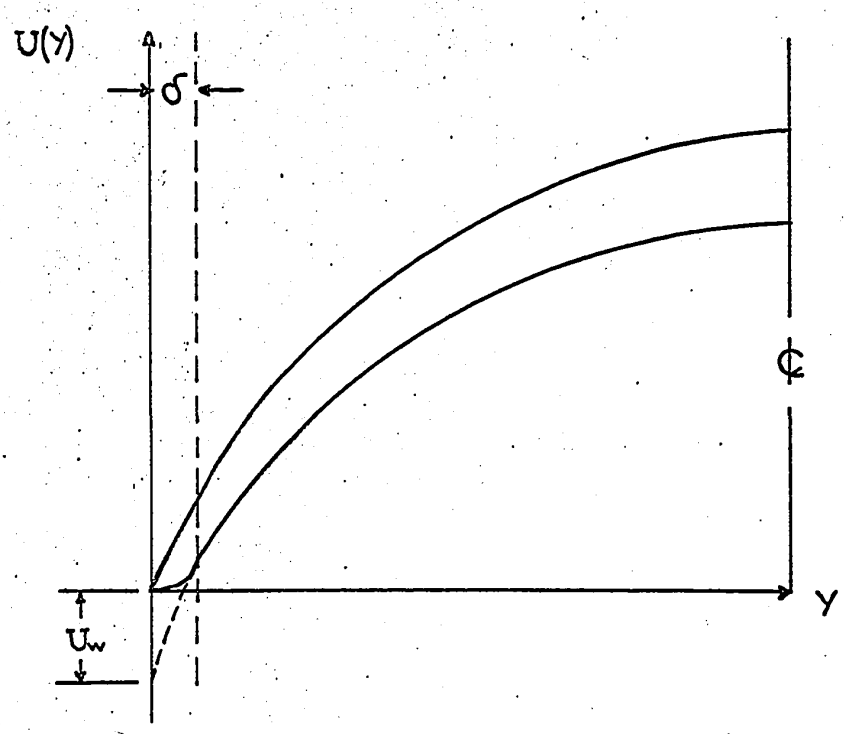


b) Negative Effective Velocity of Slip (Adsorption)

Fig. 1 Velocity Profiles Adjacent to a Solid Boundary in Laminar Flow.

## IV - VISCOMETRIC EXPERIMENTS

Among the several types of viscometers available[7] for the characterization of non-Newtonian fluids, the one which proves most useful[35], is the capillary or extrusion rheometer.

Commercial versions of this type of viscometer are available on the market[7] but it is customary to have one constructed in the laboratory shop according to the specifications of the user.

a) Capillary Viscometer

The capillary viscometer is used to measure the pressure gradient and the mass rate of flow of a liquid through a capillary tube of precisely known diameter. From those measurements, a relationship can be established between the shear rate and the shear stress of the fluid under study.

The mathematical treatment of the data so obtained can be found in Skelland[40] or in Appendix A.

The apparatus used here is characterized by the following features:

1. a fluid reservoir
2. three capillary tubes
3. pressurizing facilities
4. a thermoregulated circulating water bath.

A schematic diagram of the apparatus is shown on Fig. 2.

The reservoir is constructed from a 14.3 cm. I.D. plexiglass pipe of thickness 0.4 cm. It stands approximately 45 cm. high with two plexiglass plates glued at each end. On the bottom plate, an hexagonal nut with internal bore is fixed solidly, through which the

capillary tubes can be inserted and fastened. Standard sleeves and male glands were used for hermetic connections.

The upper plate of the rheometer has three perforations to hold the connections necessary for introducing the fluid under analysis, the compressed nitrogen by means of which pressure is applied to the system and finally a connection that leads to the mercury manometer. Tangential entrance of the nitrogen is provided in order to prevent bubbling and foaming of the solution.

Water, circulated from a constant temperature bath, goes through a reservoir, holding a supply of fluid and through a water jacket fitted around the viscometer. The constant temperature circulating equipment, supplied with an adjustable micro-set regulator was obtained from Haake Co. of Germany and gives a control sensitivity of $\pm$ 0.01°C over the entire temperature range.

In order to ensure a uniform temperature of the fluid flowing; over half the length of the capillary tubes lies inside the reservoir. Furthermore, due to the very short residence period of any portion of the fluid inside the capillary tube, the temperature rise should not be greater [12, 28, 42] than 1°C so that for all practical purposes, the flow is isothermal.

b) The Capillary Tubes

Three hypodermic needle tubings of type 304 austenic, chromium, nickel stainless steel, supplied by the Superior Tube Co. of Norristown, Pa. were used. The diameters ranged from .0260 to .0395 cm. I. D. with an L/D ratio varying between 580 and 857. The L/D ratios were chosen large enough so as to render the entrance effects as negligible as possible. A complete data table, pertaining to tube characteristics can be found here, below.

TABLE 1

Capillary Tubes Specifications

| Cap. No. | I. D. (cm) | Length (cm) | L/D |
|---|---|---|---|
| 26 | .0260 | 22.271 | 857 |
| 24 | .0287 | 17.962 | 625 |
| 22 | .0395 | 22.882 | 580 |

The tubes, because of their flexibility, were enclosed inside a rigid, protective, stainless steel jacket, welded at one end, and fitted with high pressure sleeves to ensure hermetic fitting when attached to the reservoir.

The tubes were all calibrated using distilled water flowing from a constant level reservoir and the diameters calculated from Poiseuille's formula, using three averaged readings:

$$R^4 = \frac{8 \mu L w}{\pi \Delta H \rho^2 gc} \quad \ldots\ldots\ldots\ldots\ldots\ldots \quad (37)$$

The deviations allowed, supplied by the manufacturer, ranged from -10.5% to + 5.3%. The deviations observed from the calibration of the capillary tubes were from - 3.4% to + 7.7% of the manufacturer's values.

c) Solution Characteristics and Preparation.

The non-Newtonian fluid used in our experiment is an aqueous solution of "Polyox WSR-301", a polyethylene oxide, supplied by the Union Carbide Co.

Polyox is a non-ionic homopolymer of approximate molecular weight $4 \times 10^6$ and formula $[-CH_2CH_2O-]_n$. The resin, being a polyether, forms very strong hydrogen bonds with water. This fact accounts for the solvation of polyox in water and the unusual thickening power it possesses.

In this experiment, the following procedure was followed; a 1% master solution was prepared by dissolving the appropriate weight of polymer in distilled water, over a period of approximately twenty minutes, using a magnetic stirrer. The solution was then left to stand overnight to ensure perfect homogeneity and then further diluted to the required concentration ranging from 20 to 40 PPM by 5 PPM steps.

Polyox solutions are susceptible to degradation by ultraviolet light or when subjected to high shears[29]. As a precaution, therefore, the solutions were used the day following their preparation and once circulated, were not reused[2].

The resin itself should not be stored more than one year, as degradation is likely to occur for storage periods longer than that.

The experimental procedure used was the following; for each Polyox concentration, the solution was extruded through each capillary tube over a pressure range of from 0 to 1 atmosphere as measured using a mercury manometer. At each pressure reading, three samples of fluid were collected in small vials, each over a precisely timed interval and weighed carefully. This procedure was repeated for each polymer concentration. At each fluid collection, the level of the solution in the reservoir was also noted so as to calculate the pressure head of the fluid above the tube.

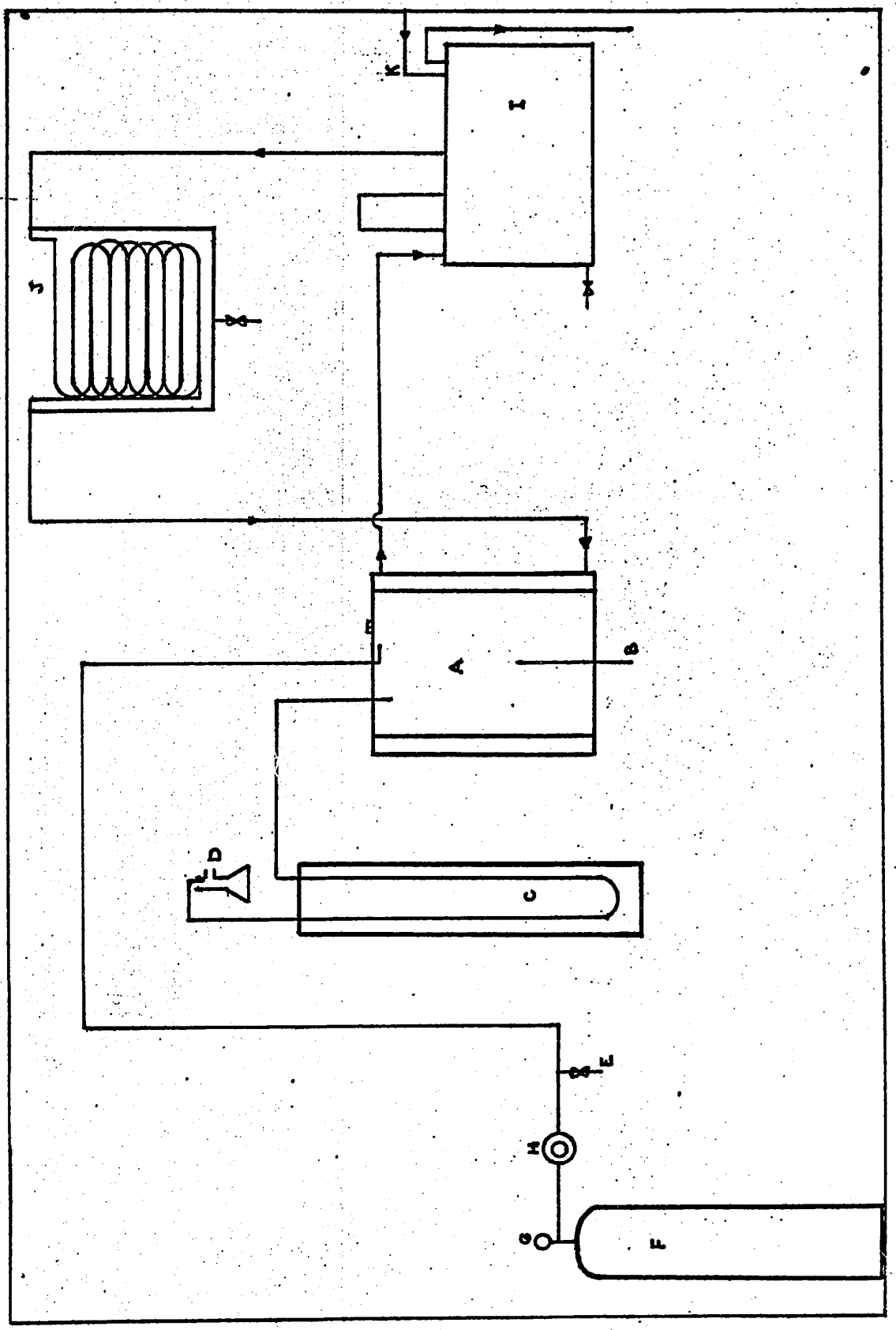


Fig. 2 Experimental Apparatus

A - Extrusion rheometer, main reservoir

B - Capillary tube

C - Mercury manometer

D - Overhead mercury spill reservoir

E - Pressure release valve

F - Nitrogen cylinder

G - Pressure regulator

H - Constant volume pressure regulator

I - Constant temperature water circulating bath

J - Overhead fluid reservoir

K - Cold water circulation

## V - RESULTS

The limited range (100-400 dynes/cm$^2$) over which the experiment was conducted in order to maintain laminar flow, permits us to draw straight lines over the data points on the shear stress - shear rate graphs.

The resolution of the diameter effect for those flow curves permits us to obtain a single line describing the exact behavior of the flowing solution when the surface effect is accounted for at a given solution concentration.

By analyzing Figs. 3 to 7 where the broken line represents the resolved flow curves, we can see that this line lies below the experimental lines thereby indicating a negative velocity of slip, i.e., polymer adsorption, at the wall of the tubes.

This is to be expected since, as was explained previously, gel-formation occurs at the vicinity of the wall at low shear-stress.

The broken line however crosses the experimental curves at a higher shear stress, if they are extended beyond the experimental region. The point of cross-over is called the critical shear-stress, $\tau_c$, and is the point where the velocity of slip changes from a negative to a positive value, corresponding, on the molecular level, to an alignment of the long polymer molecules in the direction of flow and to the formation of a thin layer of pure solvent at the wall.

Figs. 8 to 12 represent a plot of $U_w$, the negative velocity of slip versus the shear stress.

Those results are consistant with previous calculations[43] and we can observe that the curves, after rising, tend to level off and decrease and would, if extended, cross the $U_w = 0$ line at values

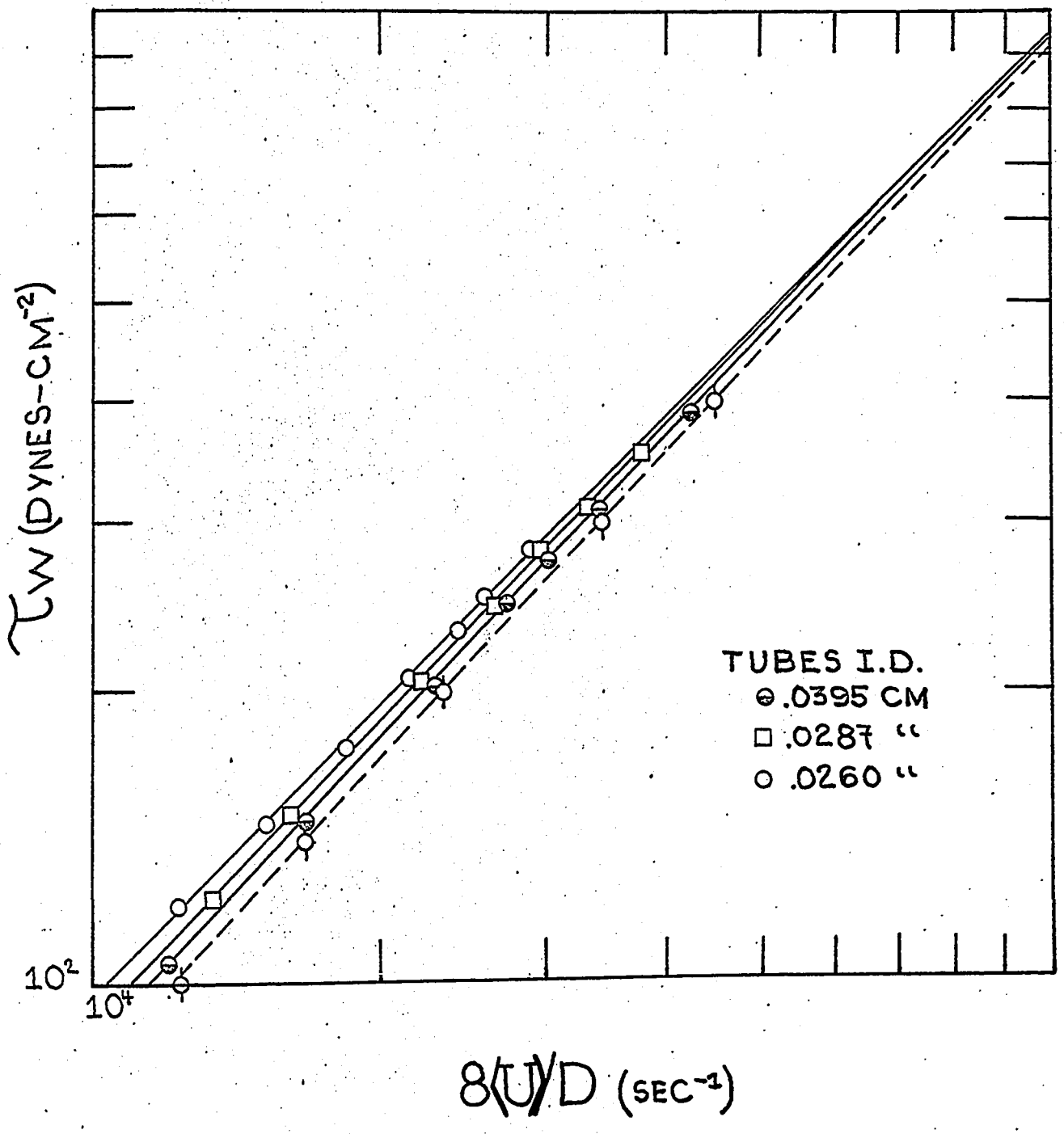


Fig. 3 Experimental and Resolved Flow Curves for a 20 ppm Polyox WSR-301 Solution

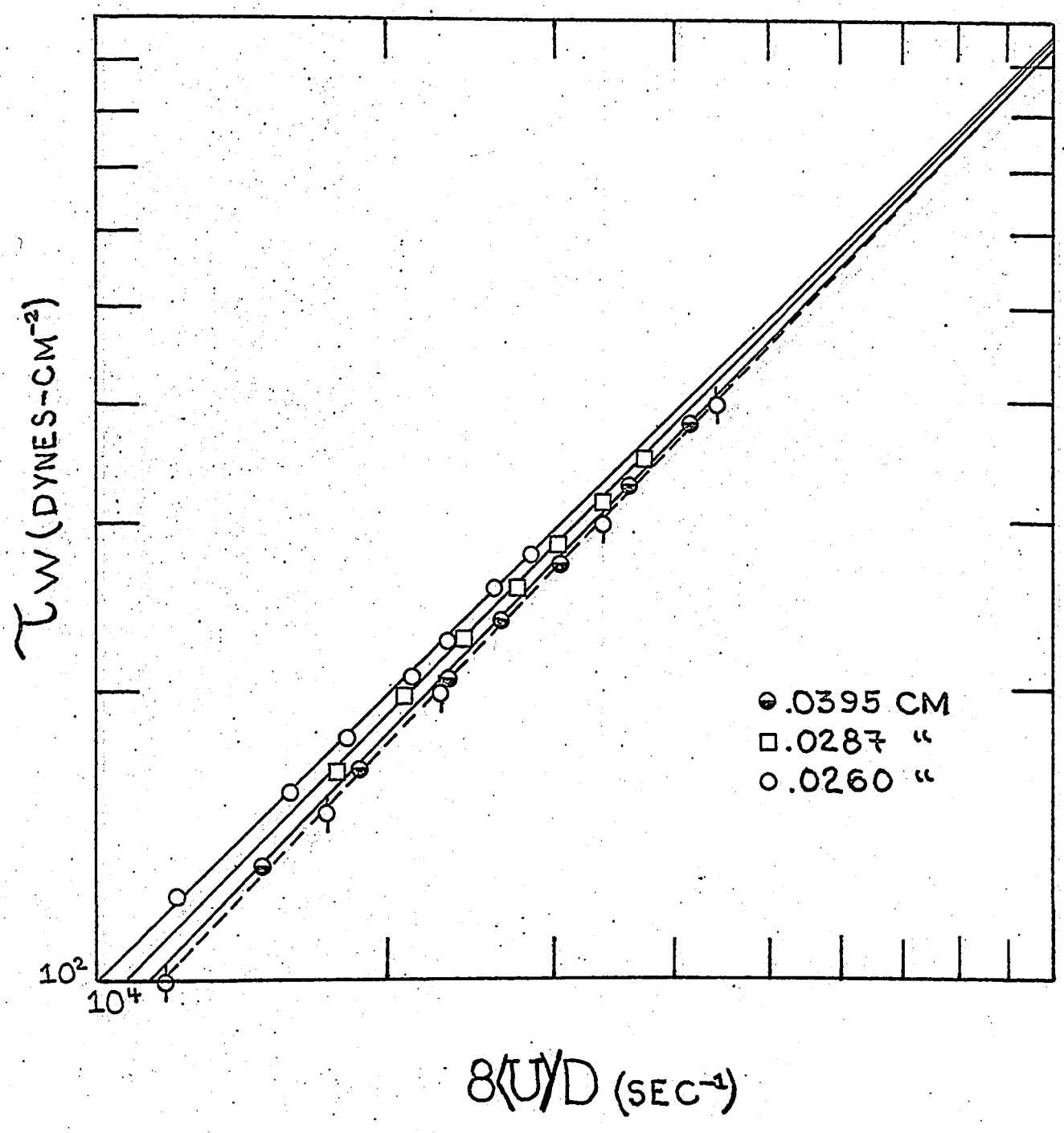


Fig. 4 Experimental and Resolved Flow Curves for a 25 ppm Polyox WSR-301 Solution

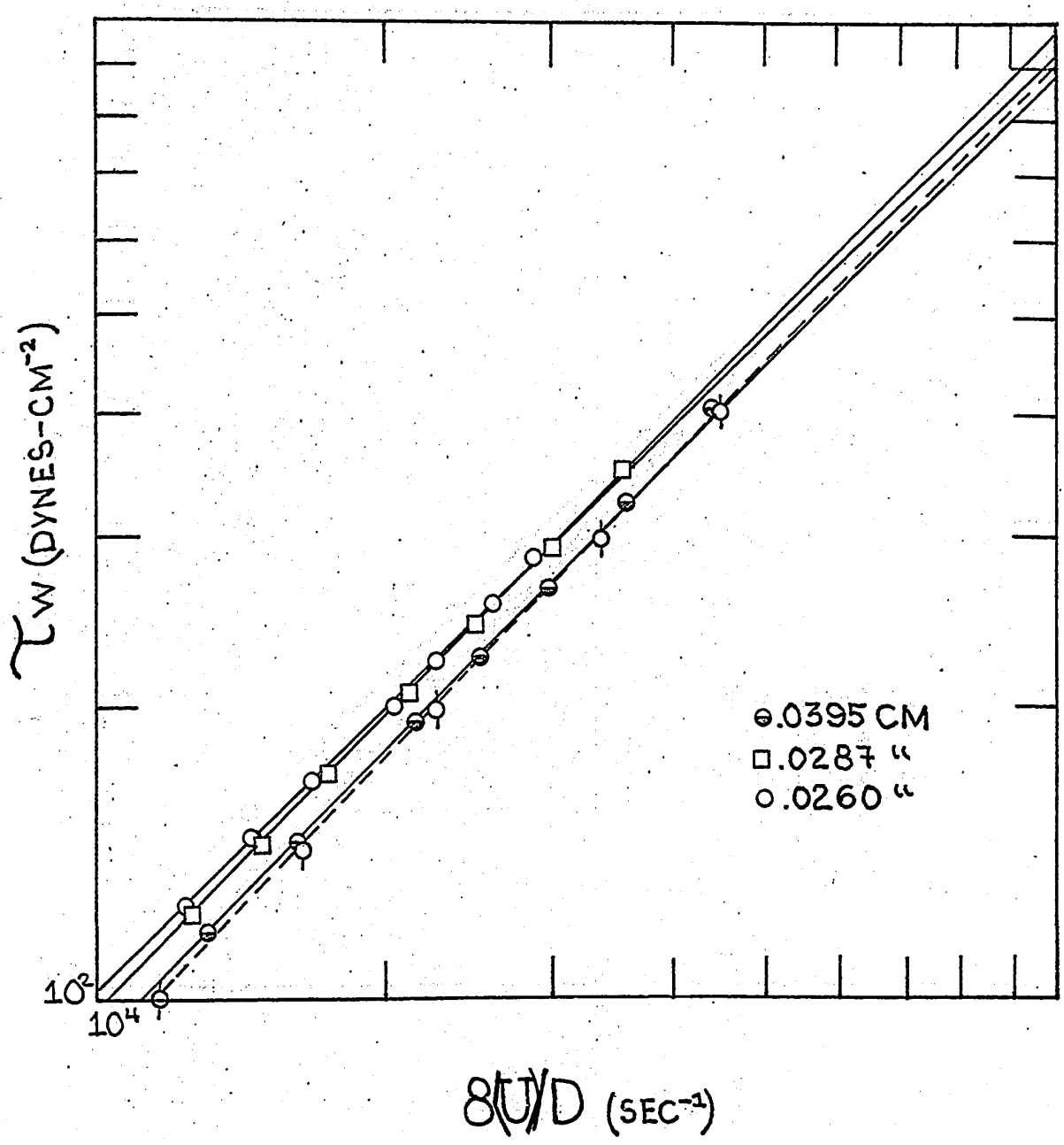


Fig. 5 Experimental and Resolved Flow Curves for a 30 ppm Polyox WSR-301 Solution

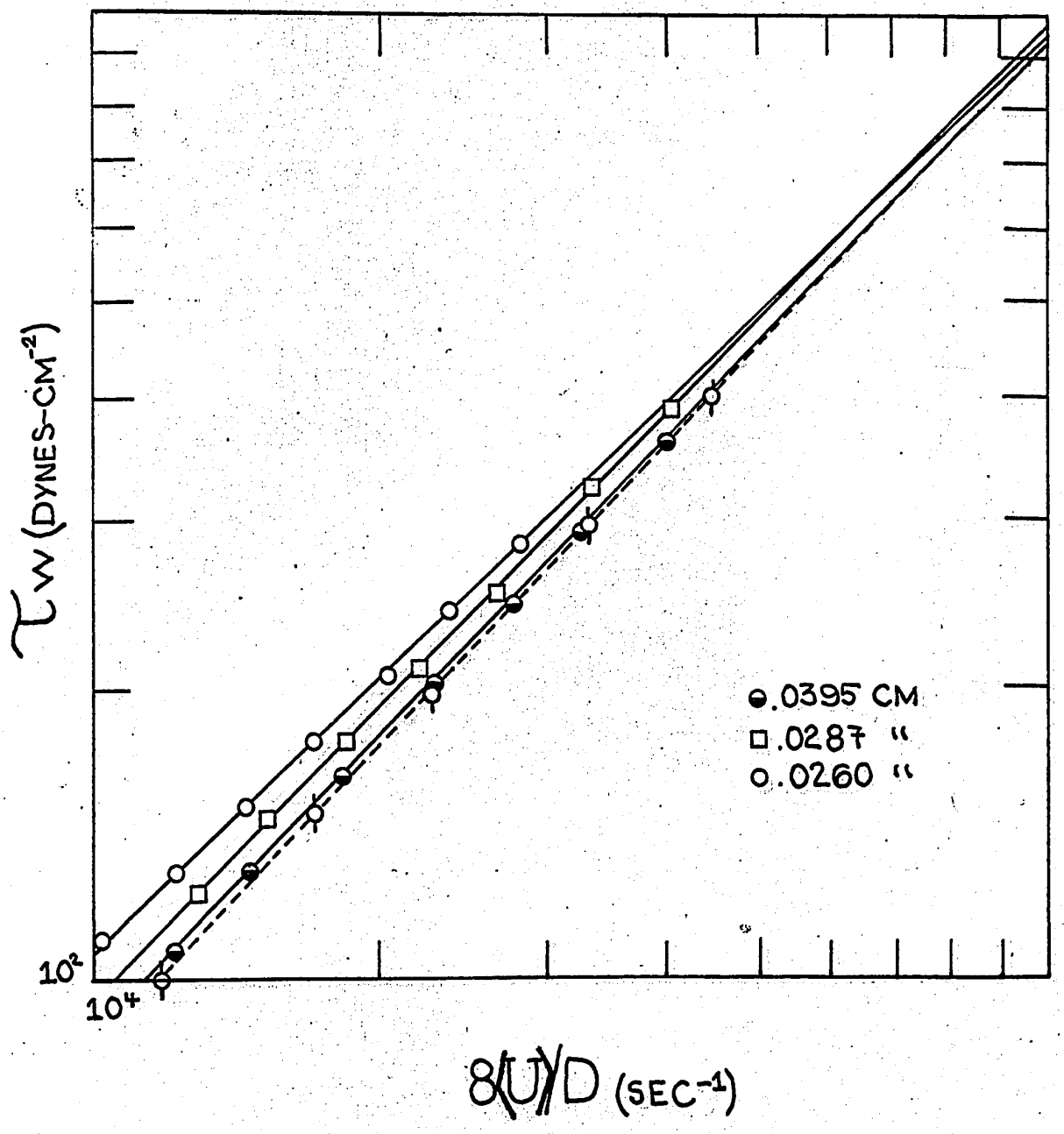


Fig. 6 Experimental and Resolved Flow Curves for a 35 ppm Polyox WSR-301 Solution

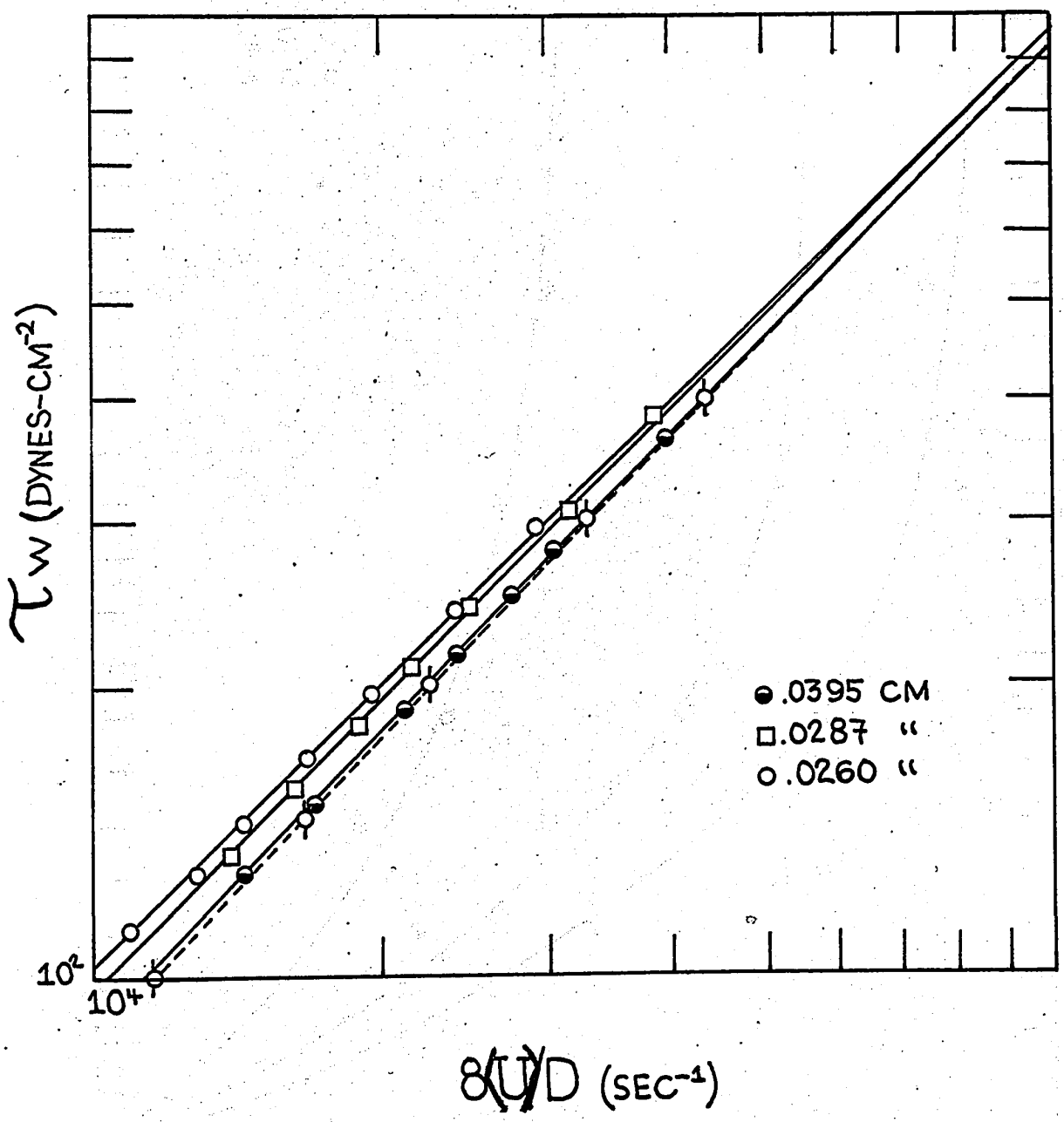


Fig. 7 Experimental and Resolved Flow Curves for a 40 ppm Polyox WSR-301 Solution

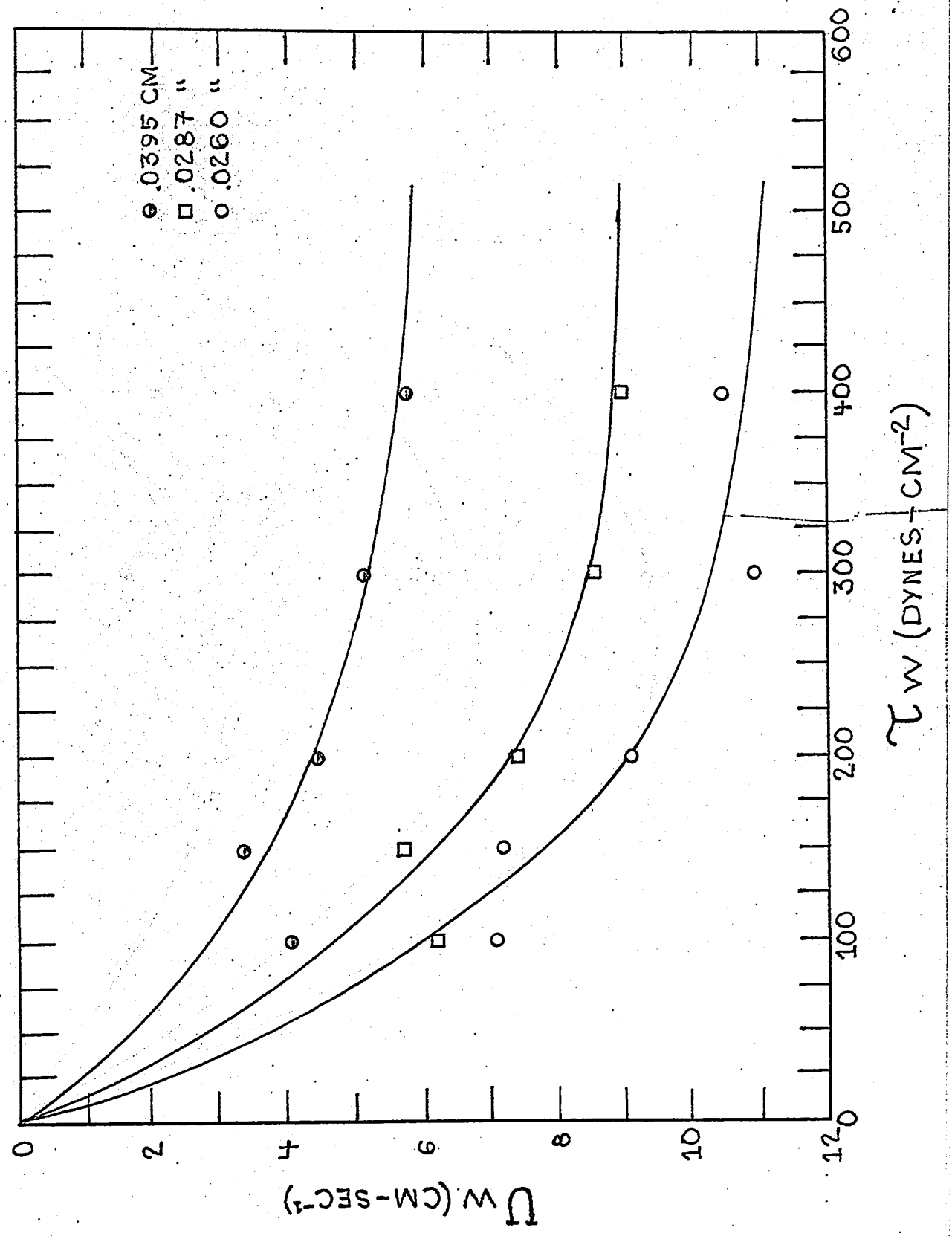


Fig. 8 Effective Velocity of Slip vs. Shear Stress for a 20 ppm Polyox WSR-301 Solution

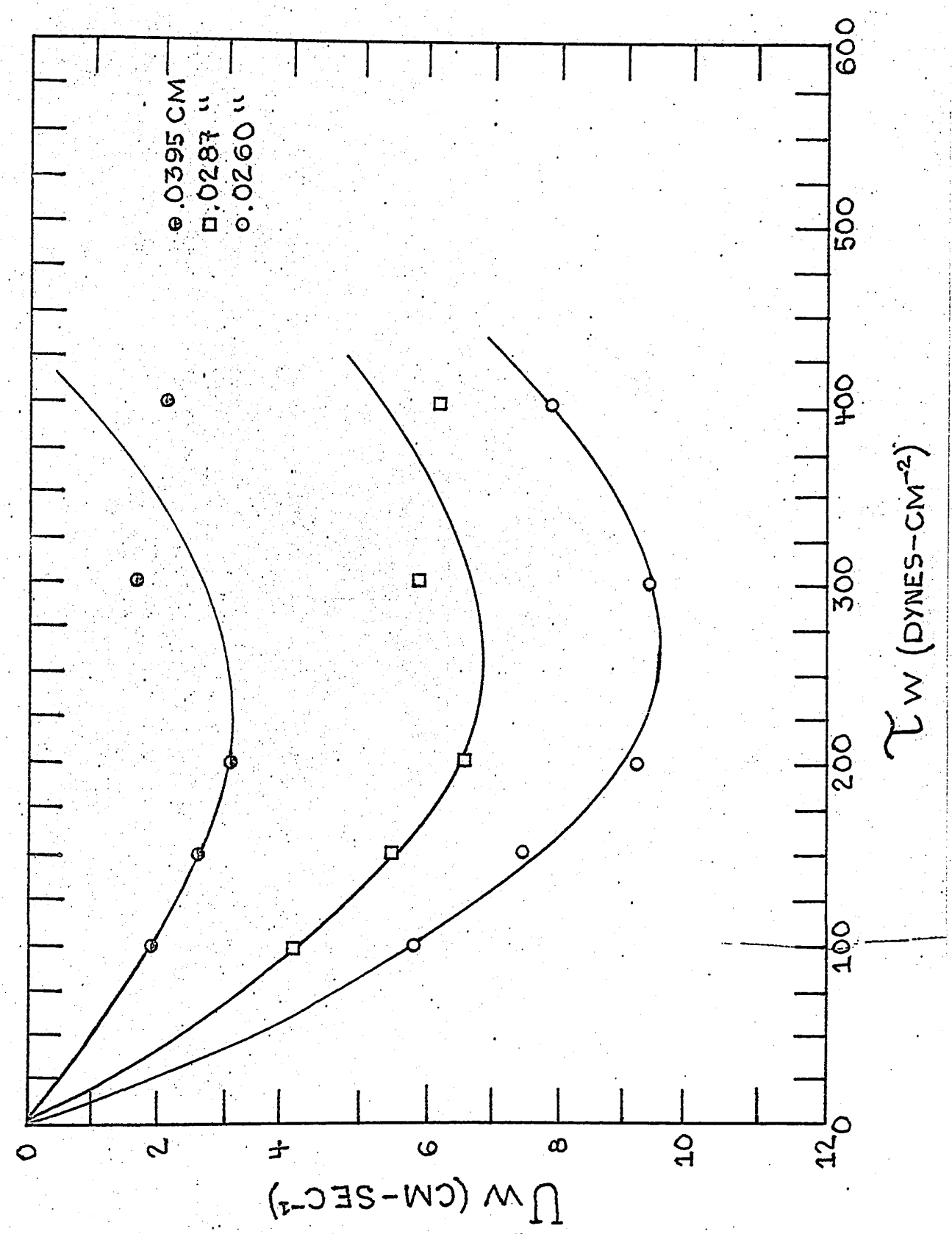


Fig. 9 Effective Velocity of Slip vs. Shear Stress for a 25 ppm Polyox WSR-301 Solution

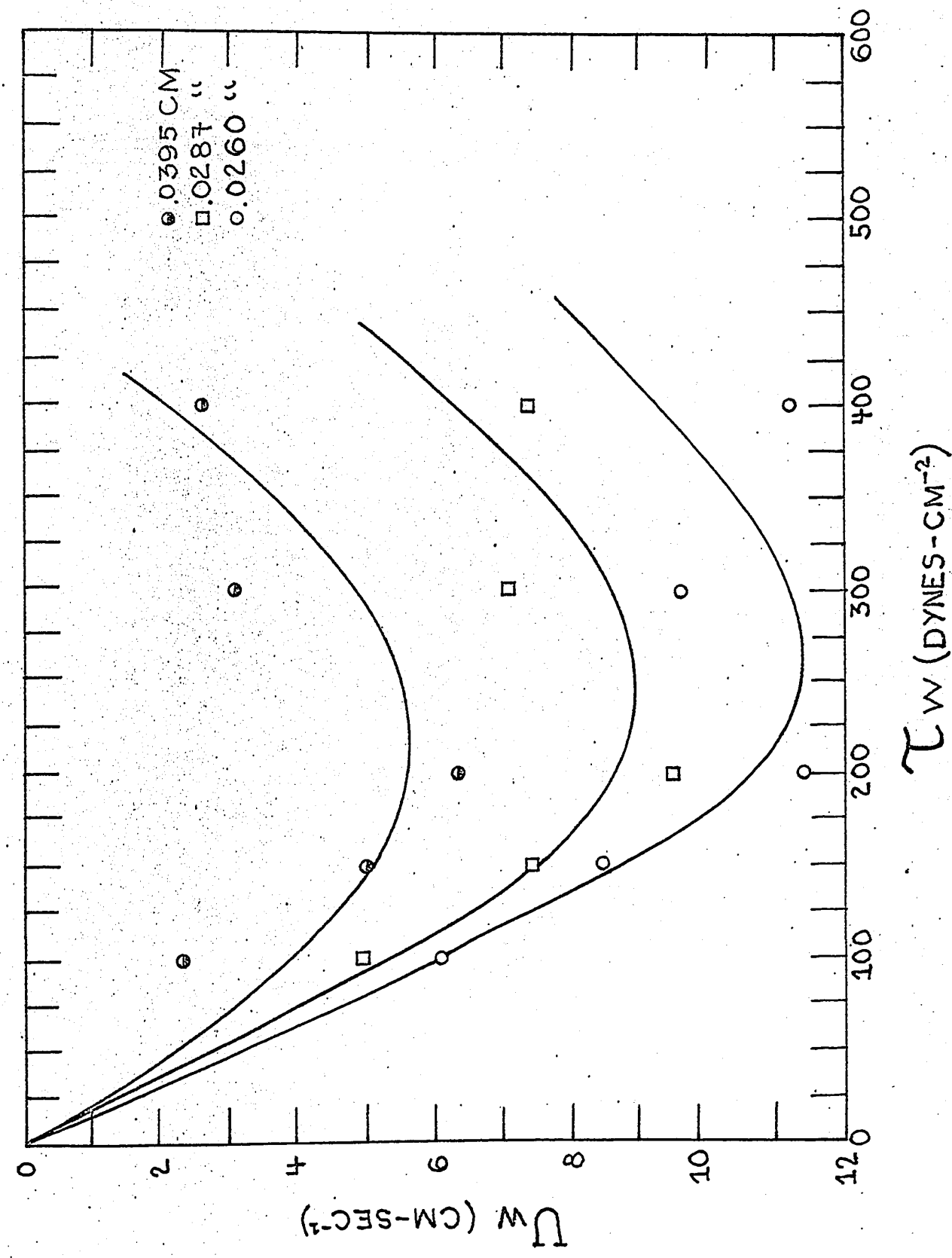


Fig. 10 Effective Velocity of Slip vs. Shear Stress for a 30 ppm Polyox WSR-301 Solution

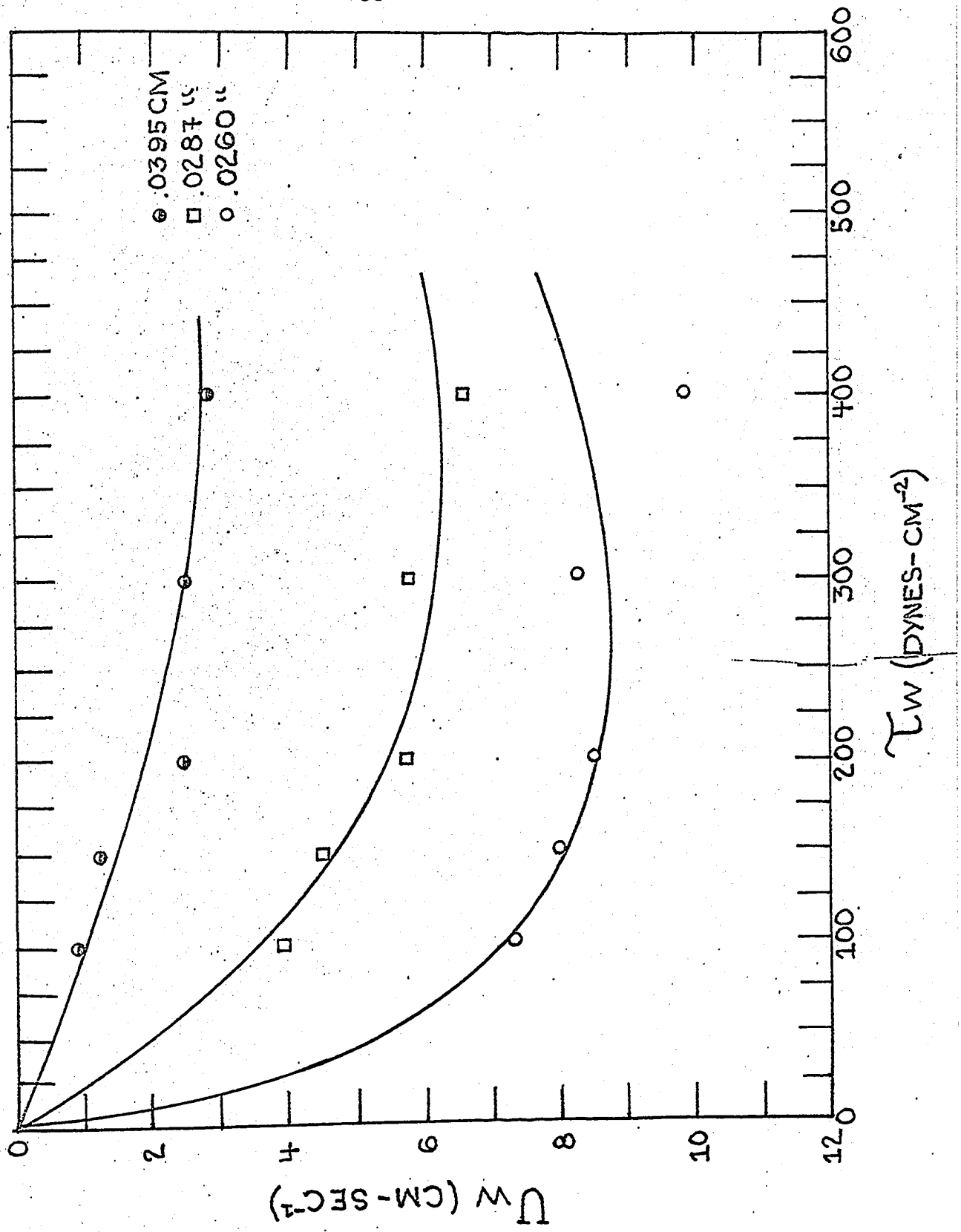


Fig. 11 Effective Velocity of Slip vs. Shear Stress for a 35 ppm Polyox WSR-301 Solution

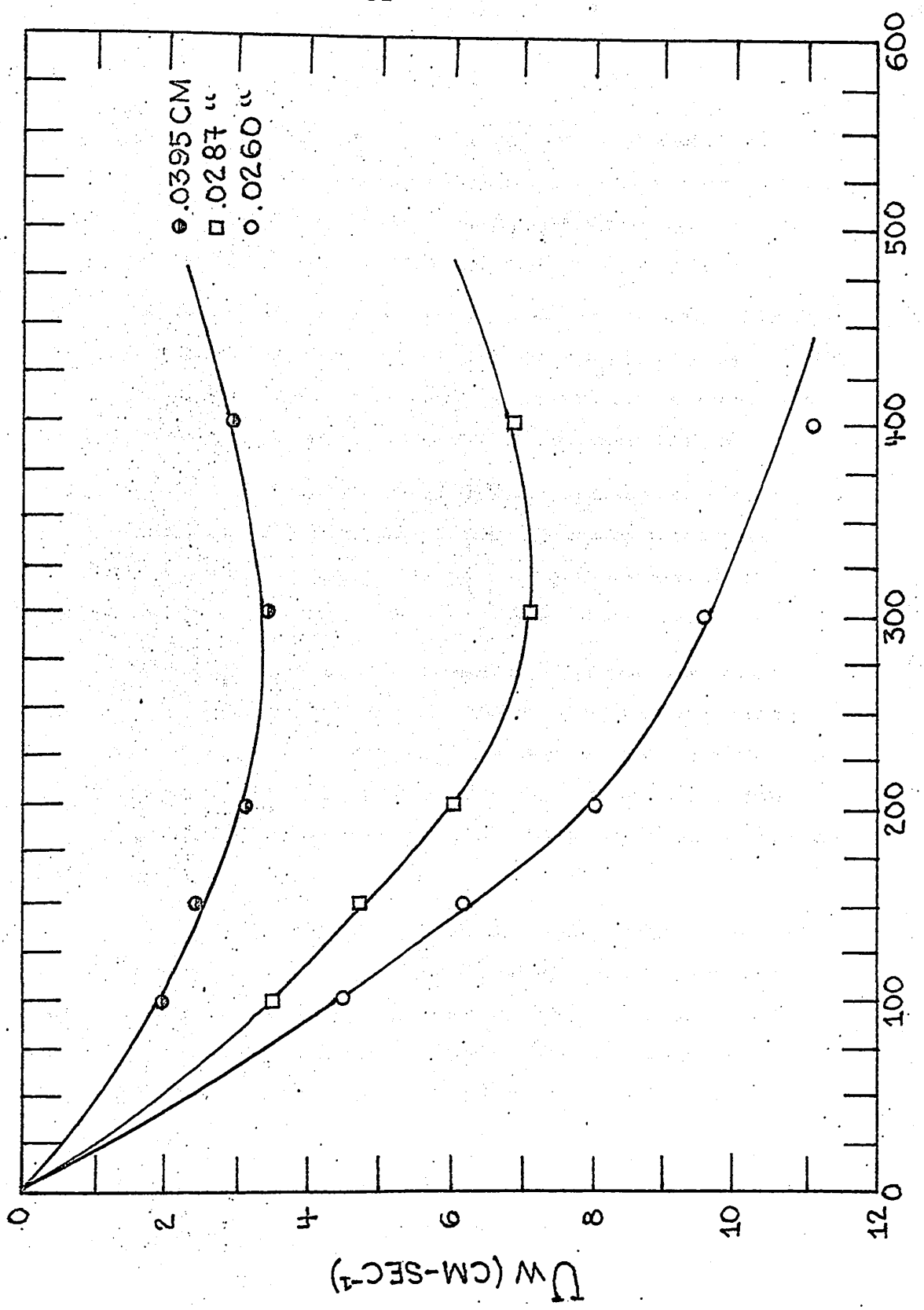


Fig. 12 Effective Velocity of Slip vs. Shear Stress for a 40 ppm Polyox WSR-301 Solution

of $\tau_w$ called the critical shear stress, $\tau_c$, as mentioned above. The slip velocity is also seen to increase, for a given shear stress and concentration value, with decreasing tube diameter, i. e., the larger the tube diameter, the smaller the slip velocity is.

The same behavior is observed if we look at Figs. 13 to 17 representing the anomalous layer thickness versus the shear stress. There, for a given shear stress and concentration, the anomalous layer thickness is largest for the smallest diameter tube used.

It serves to suggest that the anomalous behavior of drag reducing fluids, characterized by a velocity of slip at the wall, is related in some way to the formation of an anomalous layer of fluid, polymer-gel formation in this case, at the wall.

The relative value of the anomalous layer thickness at a shear stress of 100 dynes/cm$^2$, the lowest experimental value in the range studied here, varies from approximately 2. 5% of the tube diameter for the smallest tube at a concentration of 35 ppm. to a value of 0. 3% for the largest diameter tube at the same concentration and shear stress.

The anomalous layer is also behaving according to prediction, with the polymer-gel formation peeling away progressively as the shear-stress increases, till the layer thickness reaches zero at the critical shear stress defined previously. Similar results were obtained by Tiu[43] in his analysis of data collected from a wide range of workers.

From an overall comparative analysis of Figs. 8 to 12 and 13 and 17, a solution concentration of 30 ppm seems to be the optimum

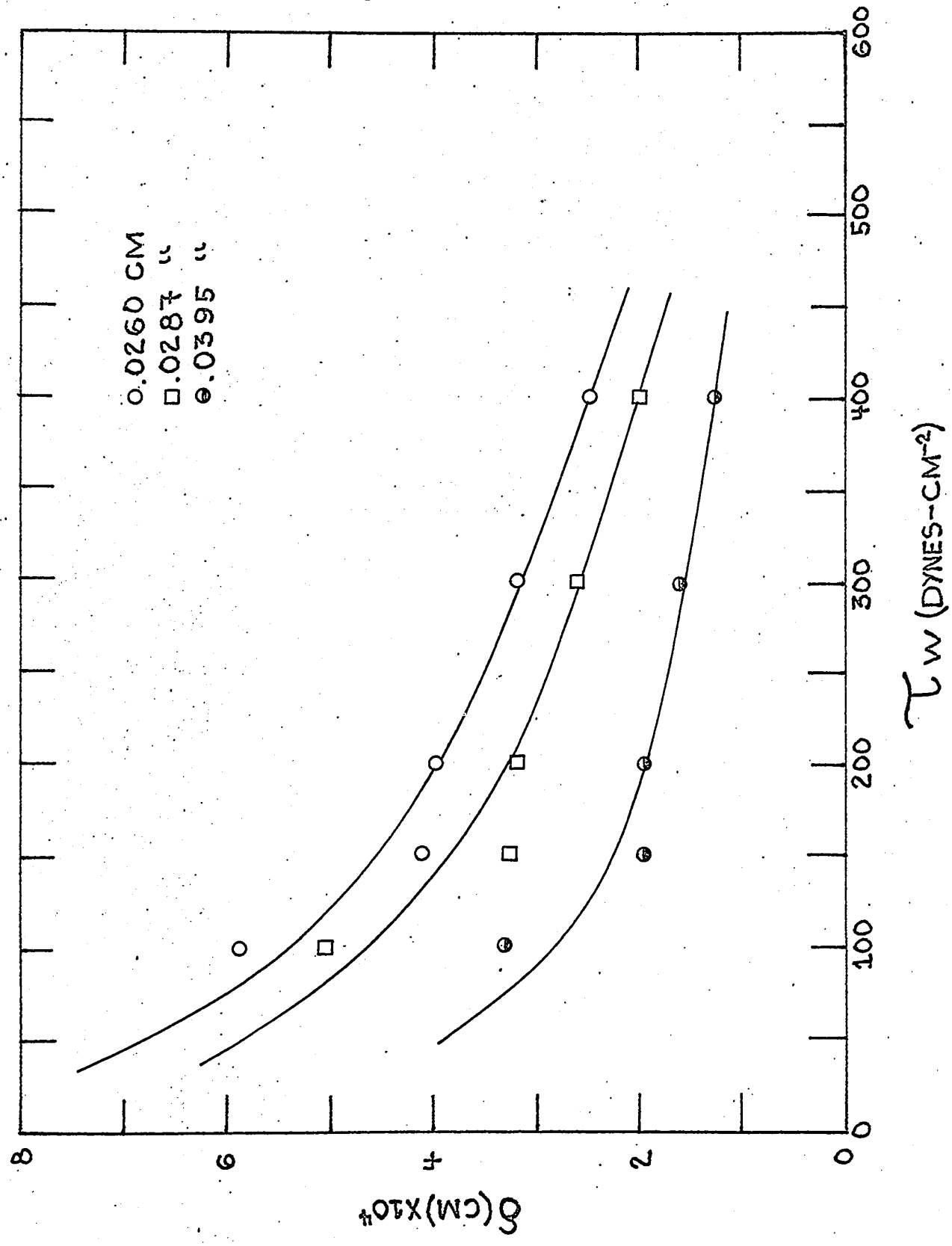


Fig. 13 Anomalous Layer Thickness vs. Shear Stress for a 20 ppm Polyox WSR-301 Solution

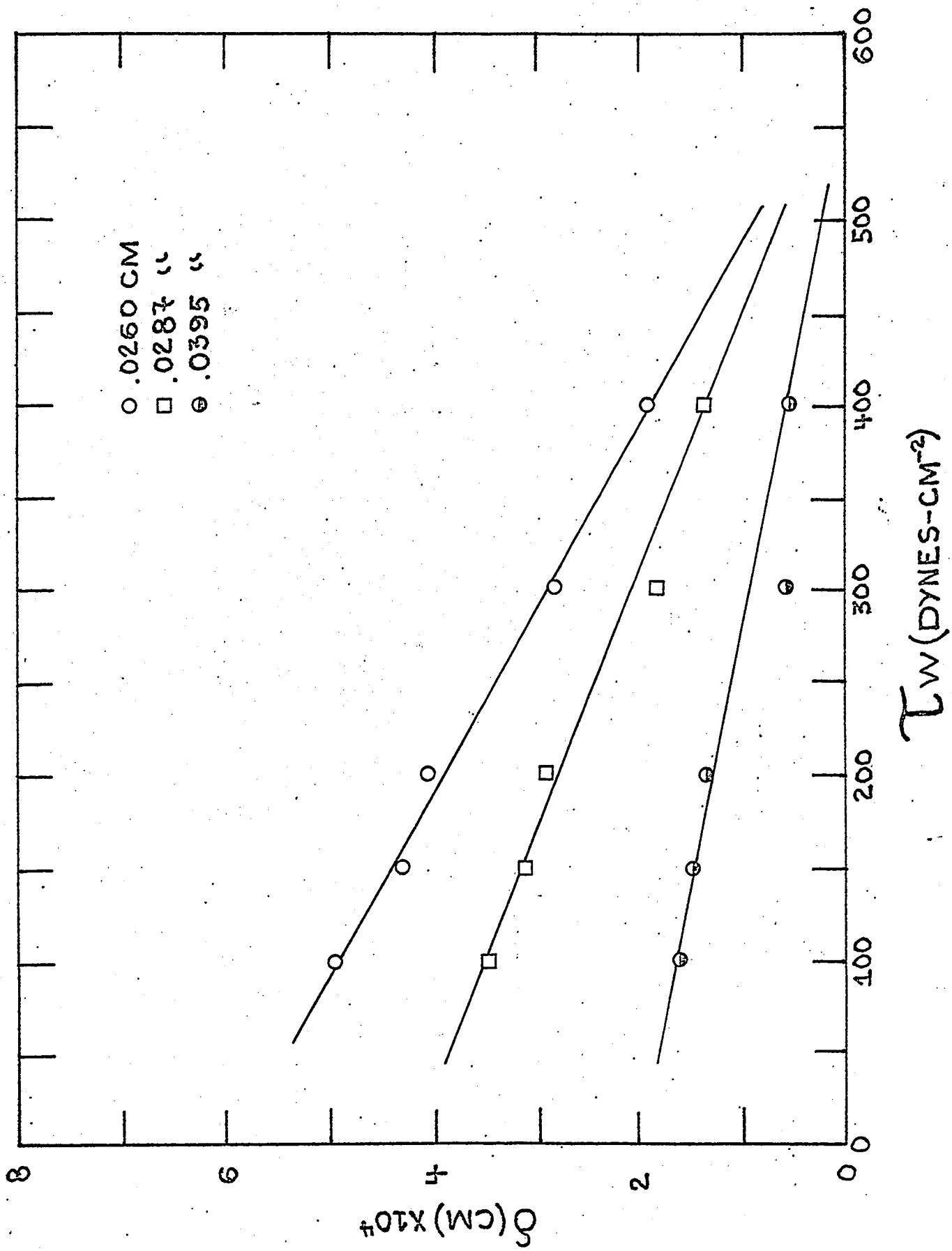


Fig. 14 Anomalous Layer Thickness vs. Shear Stress for a 25 ppm Polyox WSR-301 Solution

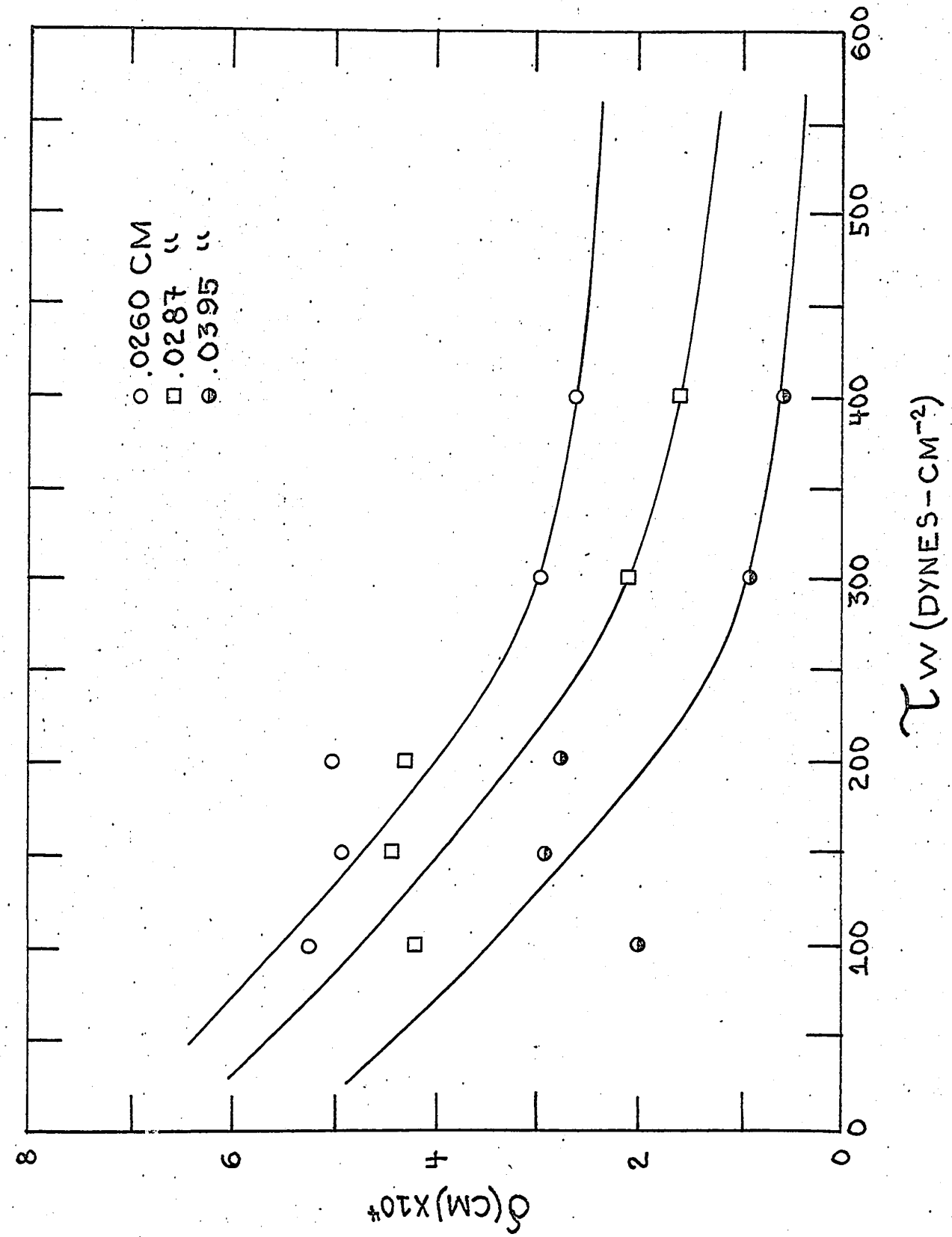


Fig. 15 Anomalous Layer Thickness vs. Shear Stress for a 30 ppm Polyox WSR-301 Solution

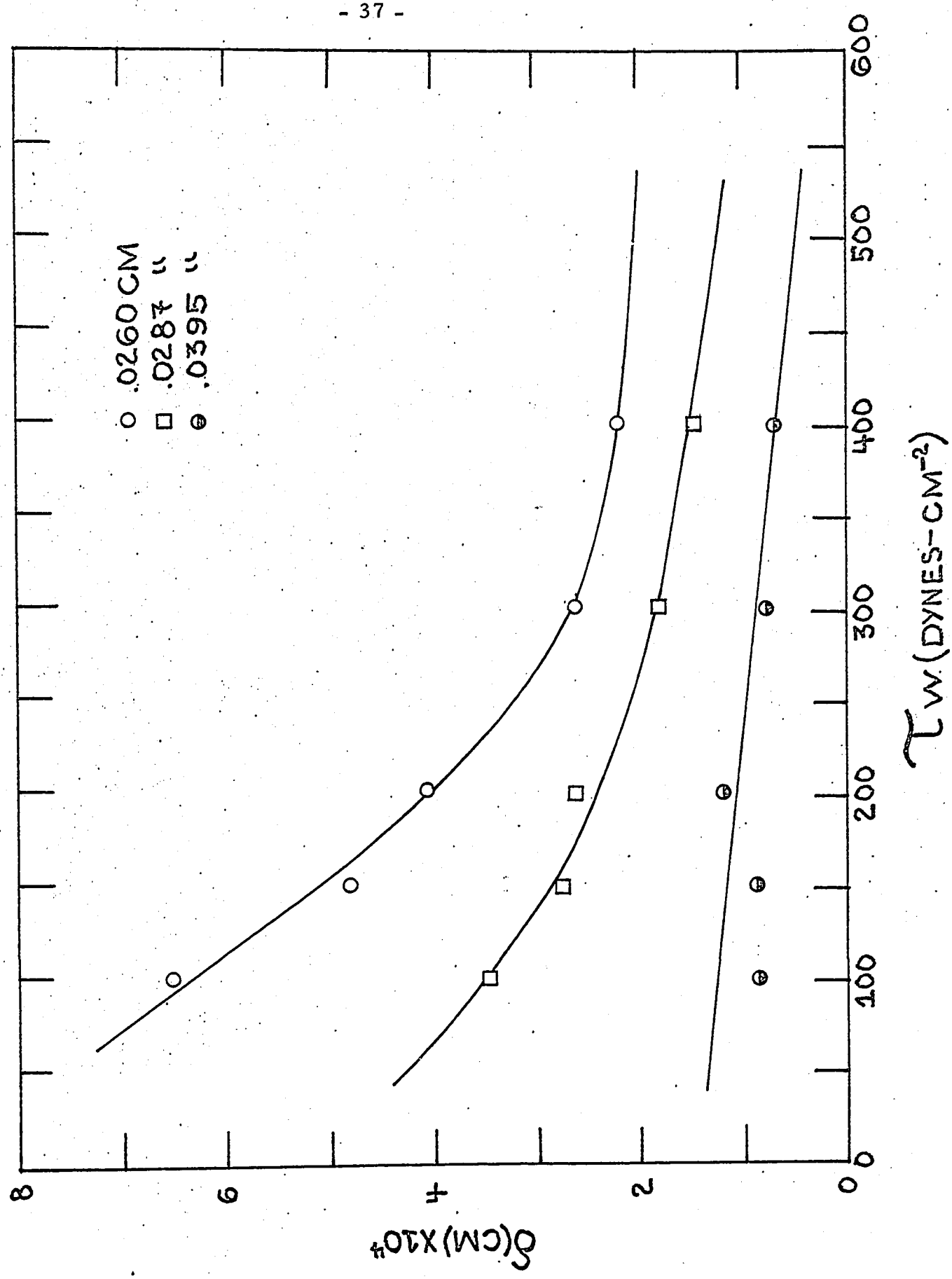


Fig. 16 Anomalous Layer Thickness vs. Shear Stress for a 35 ppm Polyox WSR-301 Solution

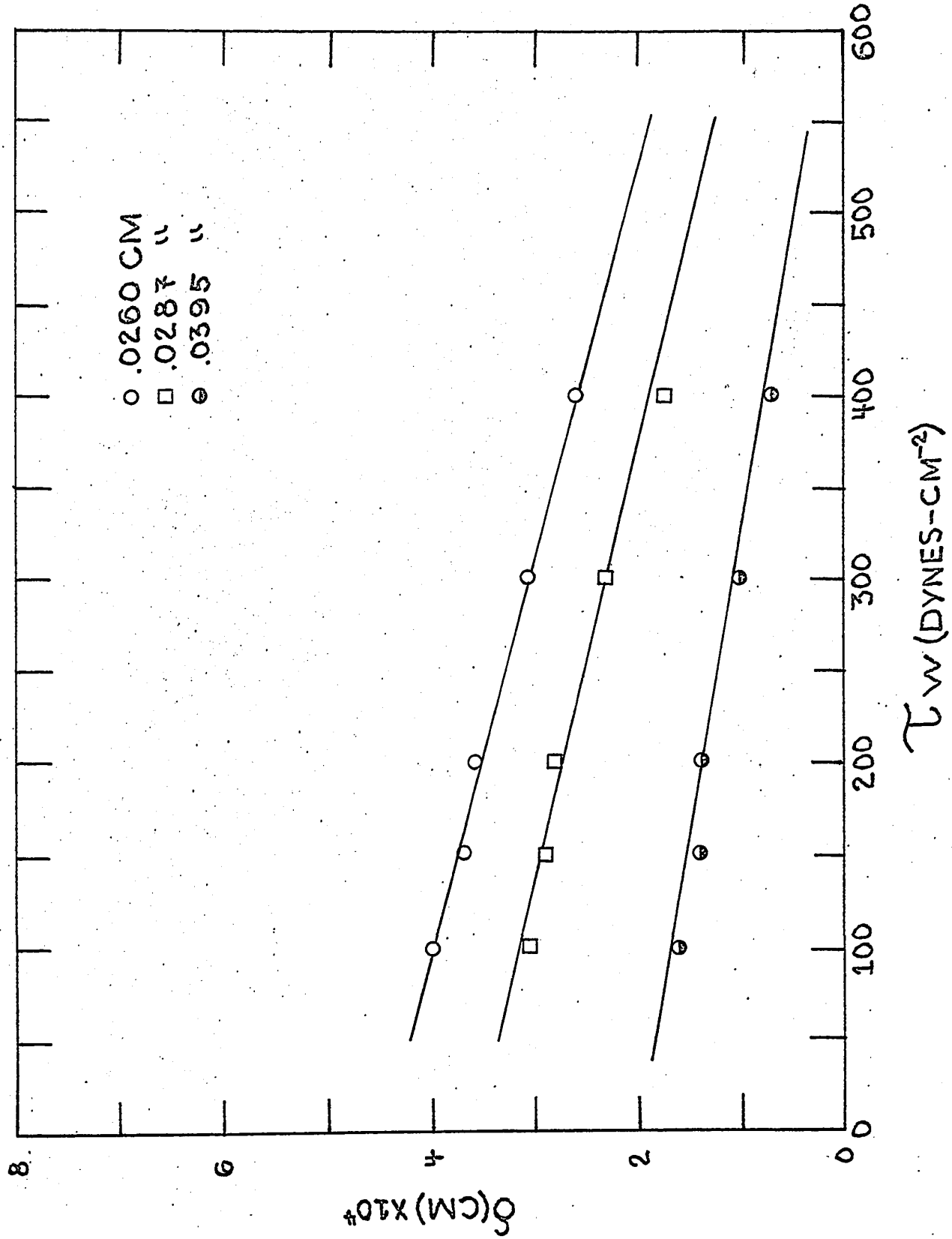


Fig. 17 Anomalous Layer Thickness vs. Shear Stress for a 40 ppm Polyox WSR-301 Solution

concentration at which the drag reducing properties of the solution reach a maximum. This is supported by previous research notably by Merrill[22] and Arunachalam[2].

## VI - CONCLUSION

In the present investigation, a method was proposed to evaluate the effective velocity of slip at the wall, for fluids exhibiting anomalous behavior at the wall.

The fluid used here, namely polyethylene oxide (Polyox WSR-301) was found to exhibit such an effect but, in the range studied, only negative values were observed which are ascribable to a polymer adsorption-gel formation phenomenon on the wall of the conduit.

The diameter effect and the concomitant effective slip velocity information were resolved using the method prescribed by Kozicki, and the different flow lines were reduced to a single line characterizing the rheological behavior of the fluid in the bulk, in laminar flow.

Anomalous layer thicknesses were evaluated and it was found that the optimum Polyox concentration in solution, in order to obtain maximum drag reduction is between 25 and 35 ppm.

The main goal of the experimentation, which was to transpose results obtained from the laminar flow of Polyox solutions to the turbulent flow of fluids exhibiting drag reduction effects was not attained.

It is therefore recommended that all future work take into careful consideration the effect of the L/D ratio on the shear stress - shear rate data in this type of experiment.

## VII - NOMENCLATURE

| | | |
|---|---|---|
| $a, b$ | = | geometric parameters (dimensionless) |
| $D$ | = | capillary tubes diameter (cm) |
| $e_v$ | = | friction loss factor (dimensionless) |
| $\hat{E}_v$ | = | total rate of viscous dissipation of mechanical energy (gm $cm^2/sec^3$) |
| $f(\tau)$ | = | shear stress function defined in Equation (6) ($sec^{-1}$) |
| $f(\tau_w)$ | = | wall shear stress function defined in Equation (12) ($sec^{-1}$) |
| $F(\tau_w)$ | = | wall shear stress function defined in Equation (18) ($sec^{-1}$) |
| $g_c$ | = | conversion factor (dimensionless) |
| $g(\tau, \delta)$ | = | correction term for the anomalous behavior in laminar flow ($sec^{-1}$) |
| $\Delta H$ | = | elevation from horizontal datum (cm) |
| $H_0$ | = | liquid head above tube (cm) |
| $K^*$ | = | fluid consistency index (gm/cm-$sec^{2-\eta'}$) |
| $L$ | = | capillary tube length (cm) |
| $\eta'$ | = | flow behavior index (dimensionless) |
| $P$ | = | isotropic pressure (cm Hg) |
| $p$ | = | potential function (gm/cm-$sec^2$) |
| $Q$ | = | volumetric rate of flow ($cm^3/sec$) |
| $r$ | = | distance from center of capillary tube (cm) |
| $R$ | = | radius of capillary tube (cm) |
| $t$ | = | time (sec) |
| $\langle U \rangle$ | = | average velocity of flow (cm/sec) |
| $U_w$ | = | effective slip velocity at the wall (cm/sec) |
| $W$ | = | sample weight (gm) |
| $\hat{W}$ | = | rate of doing work on surroundings (gm $cm^2/sec^3$) |
| $y$ | = | distance from wall of capillary tube (cm) |

GREEK LETTERS

$\alpha$ = physical parameter in Equation (A-4) (dimensionless)

$\delta$ = anomalous layer thickness (cm)

$\mu$ = viscosity (gm/cm-sec)

$\mu_s$ = solvent viscosity (gm/cm-sec)

$\Phi$ = potential energy ($gm\text{-}cm^2/sec^3$)

$\rho$ = density ($gm/cm^3$)

$\tau$ = shear stress ($dynes/cm^2$)

$\tau c$ = critical shear stress ($dynes/cm^2$)

$\tau_w$ = wall shear stress ($dynes/cm^2$)

## VIII - BIBLIOGRAPHY


1. Agoston, G. A. et al., I.& EC 46, 1017 (1954).
2. Arunachalam, V. R., Ph. D. Thesis, Univ. of Waterloo (1969).
3. Astarita, G., I & EC (Fund.) 4, 354 (1965).
4. Astarita, G., G. Greco and L. Nicodemo, A. I. Ch. E. J., 15, 565 (1969).
5. Berman, N. S., A. I. Ch. E. J., 15, 137 (1969).
6. Bird, R. B., W. E. Stewart and E. N. Lightfoot, "Transport Phenomena", 1st Ed. p. 212, John Wiley and Sons, Inc. (1966) N. Y.
7. Bowen, R. L., Chem. Eng., Aug. 21st (1961).
8. Dodge, D. W. and A. B. Metzner, A. I. Ch. E. J., 5, 189 (1959).
9. Elata, C. and J. Tirosh, Proc. VII Israel Amer. Conf. Avia & Astro. Israel J. Tech., 5, 1 (1965).
10. Ernst, W. D., A. I. Ch. E. J., 12, 581 (1966).
11. Ernst, W. D., A. I. A. A. J., 5, 906 (1967).
12. Gerrand, I. E. et al., I & EC (Fund.) 5, 261 (1966).
13. Goren, Y. and J. F. Norbury, Trans. ASME 89D, 814 (1967).
14. Haynes, R. H., Trans. Soc. Rheol. V, 85 (1961).
15. Hershey, H. and J. L. Zakin, Symposium on Mechanics of Viscoelastic Fluids, Part II, 58th Annual Meeting (1965).
16. Hershey, H. and J. L. Zakin, I & EC (Fund.) 6, 381 (1967).
17. Hoyt, J. W. and A. G. Fabula, 5th Symp. Naval Hydrodynamics, Bergmen, Norway (1964).
18. Jastrzebski, Z. D., I & EC (Fund.) 6, 445 (1967).
19. Kozicki, W., J. Hsu and C. Tiu, Chem. Eng. Sci., 22, 487 (1967).
20. Kozicki, W. and C. Tiu, Can. J. Chem. Eng., 45, 127 (1967).

21. Kozicki, W. and C. Tiu, Chem. Eng. Sci., 23, 231 (1968).

22. Merril, E. W., K. A. Smith and R. Y. C. Chung, A.I. Ch. E. J., 12, 809 (1966).

23. Metzner, A. B. and G. Park, J. Fluid Mech., 20, 291 (1964).

24. Mooney, M., J. Rheo., 2, 210 (1931).

25. Mooney, M., J. Rheo., 2, 337 (1931).

26. Oldroyd, J. F., J. Colloid. Sci., 4, 333 (1949).

27. Oliver, D. R. and W. MacSporran, Can. J. Chem. Eng., 46, 233 (1968).

28. Pasari, S. N., Master's Thesis, Univ. of Ottawa (1968).

29. Paterson, R. W. and F. H. Abernathy, J. Fluid Mech., 43, 689 (1970).

30. Patterson, G. K., J. L. Zakin and J. M. Rodriguez, I & EC (Fund.) 61, 22 (1969).

31. Rabinowitsch, B. Z., Phys. Chem., A145, 1 (1929).

32. Sadowski, T. J., Ph. D. Thesis, Univ. of Wisconsin (1963).

33. Savins, J. G., J. Inst. Petrol., 47, 329 (1961).

34. Schofield, R. K. and W. S. Blair, J. Phys, Chem., 34, 248 (1930).

35. Severs, E. T. and J. M. Austin, I & EC 46, 2369 (1954).

36. Seyer, F. A., J. Fluid Mech., 40, 807 (1970).

37. Seyer, F. A. and A. B. Metzner, A. I. Ch. E. J., 15, 427 (1969).

38. Seyer, F. A. and A. B. Metzner, Can. J. Chem. Eng., 47, 525 (1969).

39. Shaver, R. G. and E. W. Merril, A. I. Ch. E. J., 5, 181 (1959).

40. Skelland, A. H. R., "Non-Newtonian Flow and Heat Transfer", 1st Ed. (1967) John Wiley & Sons, Ltd., N. Y.

41. Tiu, C., Ph. D. Thesis, Univ. of Ottawa (1968).

42. Toms, B. A., Proc. Int. Cong. Rheol. II, p. 135, North Holland Publishing Co. Amsterdam (1949).

43. Toor, H. L., Trans. Soc. Rheol. 1, 177 (1957).

44. Virk, P. S. et al., J. Fluid Mech., 30, 305 (1967).

45. Wells, C. S., Am. Inst. Aero. Astro. J., 3, 1800 (1965).

46. Wells, C. S. and J. G. Spangler, Phys. Fluids, 10, 1890 (1967).

# APPENDICES

# APPENDIX A

## DETAILED SET OF CALCULATIONS

## Detailed Set of Calculations

In order to demonstrate clearly the mathematical developments involved in obtaining the stated results, we will follow here, for a 20 ppm concentration, the various steps used:

The mechanical energy equation for a steady state system can be written as[6]:

$$\Delta \tfrac{1}{2} \frac{\langle U^3 \rangle}{\langle U \rangle} + \Delta \bar{\Phi} + \int_0^1 1/\rho \; dp + \hat{W} + \hat{E}_v = 0 \quad \ldots\ldots\ldots \text{(A-1)}$$

in reference to Fig. A-1

In our case, $W = 0$ and $\Delta \bar{\Phi} = g \Delta H$ so that Equation (A-1) can be written as:

$$\Delta \tfrac{1}{2} \frac{\langle U^3 \rangle}{\langle U \rangle} + g \Delta H + \int_0^1 1/\rho \; dP + E_v = 0 \quad \ldots\ldots\ldots \text{(A-2)}$$

since we assume that the liquid is incompressible:

$$\int_0^1 1/\rho \; dP = \frac{1}{\rho} (P_1 - P_0) \quad \ldots\ldots\ldots\ldots\ldots\ldots \text{(A-3)}$$

and the first term in Equation (A-2) can be written as[40]:

$$\Delta \tfrac{1}{2} \frac{\langle U^3 \rangle}{\langle U \rangle} = \tfrac{1}{2} \frac{\langle U \rangle^2}{a} \quad \ldots\ldots\ldots\ldots\ldots\ldots \text{(A-4)}$$

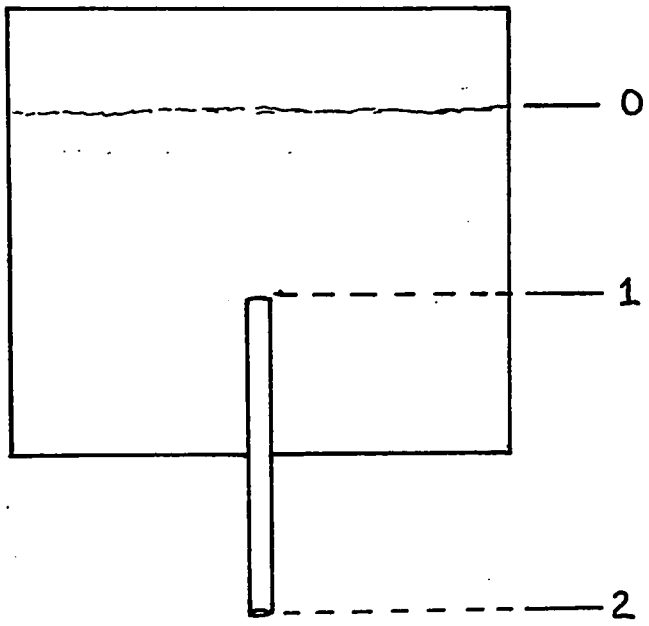


Fig. A-1 Mechanical Energy Balance Diagram

then Equation (A-2) becomes:

$$\frac{1}{2}\frac{\langle U\rangle^2}{\alpha} + g\,(H_1 - H_0) + \frac{1}{\rho}\,(P_1 - P_0) + \frac{1}{2}\langle U_1\rangle^2 e_v = 0 \qquad \text{..... (A-5)}$$

now, if we let:

$$P_0 = p_0 + \rho\, g\, H_0$$
$$P_1 = p_1 + \rho\, g\, H_1 \qquad \text{..... (A-6)}$$

and replace Equation (A-6) into (A-5), we obtain

$$\frac{1}{\rho}\,(P_1 - P_0) + \frac{1}{2}\langle U_1\rangle^2 \left[\frac{1}{\alpha} + \rho_v\right] = 0 \qquad \text{..... (A-7)}$$

from Skelland[40]:

$$\frac{1}{2}\left[\frac{1}{\alpha} + \rho_v\right] = 1.12 \qquad \text{..... (A-8)}$$

and Equation (A-7) finally becomes:

$$p_1 = p_0 - 1.12\ \rho\ \langle U \rangle^2 \quad \ldots\ldots\ldots\ldots\ldots\ldots\ (A\text{-}9)$$

now, for the system represented in Fig. A-1, the mechanical energy balance becomes:

$$p_1 - p_2 = p_0 - p_2 - 1.12\ \rho\ \langle U \rangle^2 \quad \ldots\ldots\ldots\ldots\ (A\text{-}10)$$

and knowing that

$$\tau_w = \frac{D}{4}\left[\frac{p_1 - p_2}{L}\right] \quad \ldots\ldots\ldots\ldots\ldots\ldots\ (A\text{-}11)$$

then, rearranging Equation (A-10) and replacing Equation (A-11) into it, we obtain:

$$\tau_w = \frac{D}{4}\left[\frac{\Delta P}{L} + \frac{H_0 + L}{L}\ \rho - \frac{1.12\ \rho\ \langle U \rangle^2}{L\, g_c}\right] \quad \ldots\ (A\text{-}12)$$

which is the equation used to calculate $\tau w$ from the experimental measurements.

The shear rate $8\ \langle U \rangle / D$ is calculated from the following development:

$$\langle U \rangle = \frac{W}{\rho\, A\, t} \quad \ldots\ldots\ldots\ldots\ldots\ldots\ (A\text{-}13)$$

the cross-section area of the tube A, can be written as:

$$A = \frac{\pi D^2}{4} \quad \ldots\ldots\ldots\ldots\ldots\ldots\ (A\text{-}14)$$

so that the shear rate becomes:

$$\frac{8\ \langle U \rangle}{D} = \frac{32\ W}{\pi\ \rho\ D^3\ t} \quad \ldots\ldots\ldots\ldots\ (A\text{-}15)$$

So much for the calculations of $\tau_w$ and 8 $\langle U \rangle / D$, the shear stress and the shear rate respectively.

We now proceed to calculate $U_w$, the effective velocity of slip, and 8 $(U-U_w)/D$, the shear rate corrected for the diameter and slip effects.

From Fig. A-2, we choose five different values of $\tau w$ and read off the corresponding 8 $\langle U \rangle / D$ values on each tube diameter curve.

The 8 $\langle U \rangle / D$ values so obtained are plotted against the 1/D values on Fig. A-3 and the slopes $\partial (8 \langle U \rangle / D) \partial (1/D)$, at the three 1/D values corresponding to the tube diameters used in our experiment, are calculated from the graph, at each $\tau_w$ value.

A second plot is then prepared with the slopes ploted vs. the 1/D values as in Fig. A-4, for each $\tau_w$ value. So that from Fig. A-4, we just have to evaluate the appropriate areas under the curve in order to obtain $U_w$, the effective slip velocity.

Once $U_w$ is obtained, it is easy to calculate the corresponding 8 $(\langle U \rangle - U_w)/D$ values and plot the final flow curves which appear as dotted lines on Figs. 3 to 7.

The complete results for a 20 ppm solution are compiled in Table A-1.

The second important result that we find is the anomalous layer thickness $\delta$. It is obtained from the following set of equations which were developed previously:

$$\delta = - U_w / f(\tau_w) \quad \ldots\ldots\ldots\ldots\ldots\ldots\ldots\ldots \quad (A\text{-}16)$$

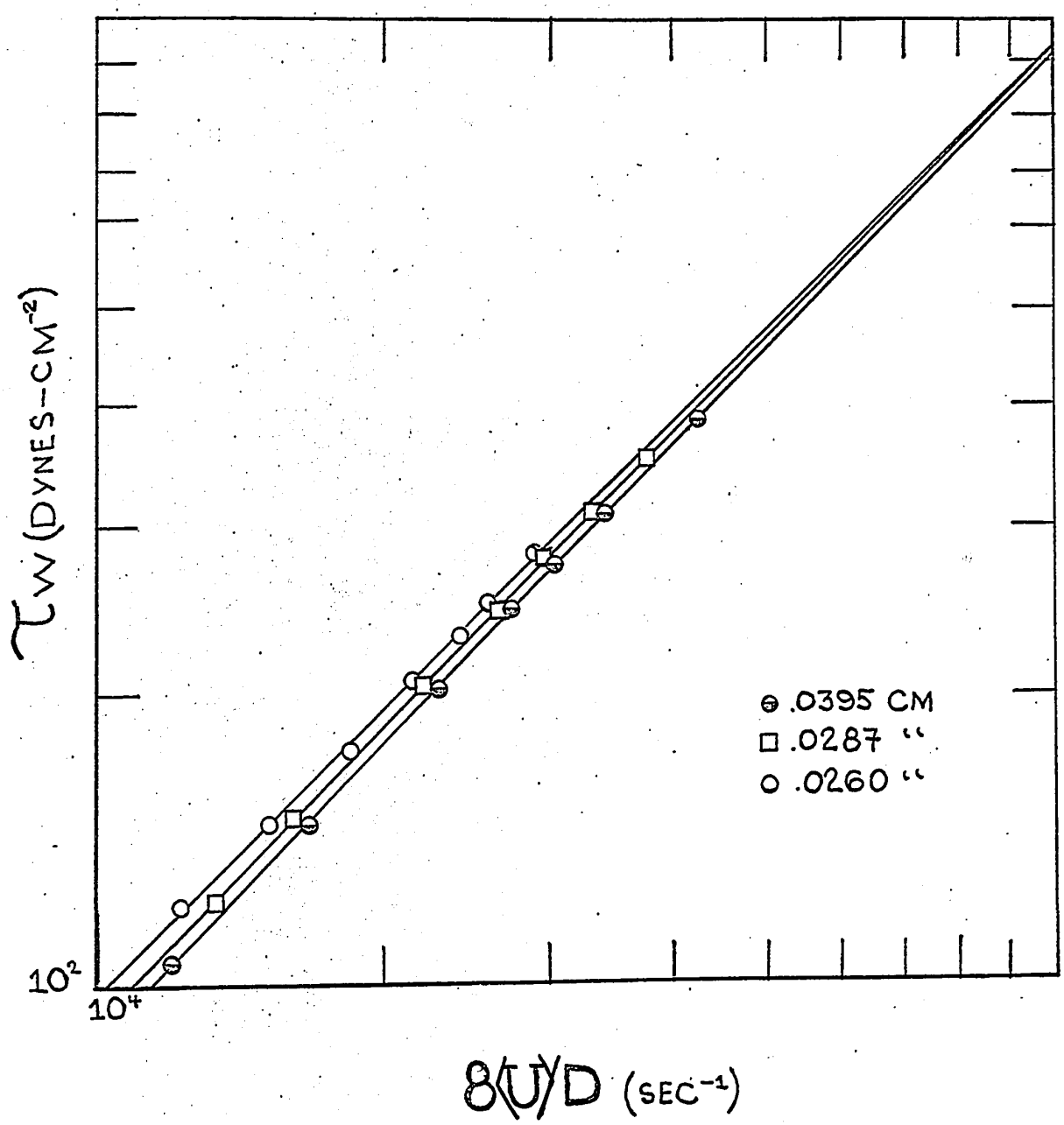


Fig. A-2 Shear Stress vs. Shear Rate Plot for a 20 ppm Polyox WSR-301 Solution

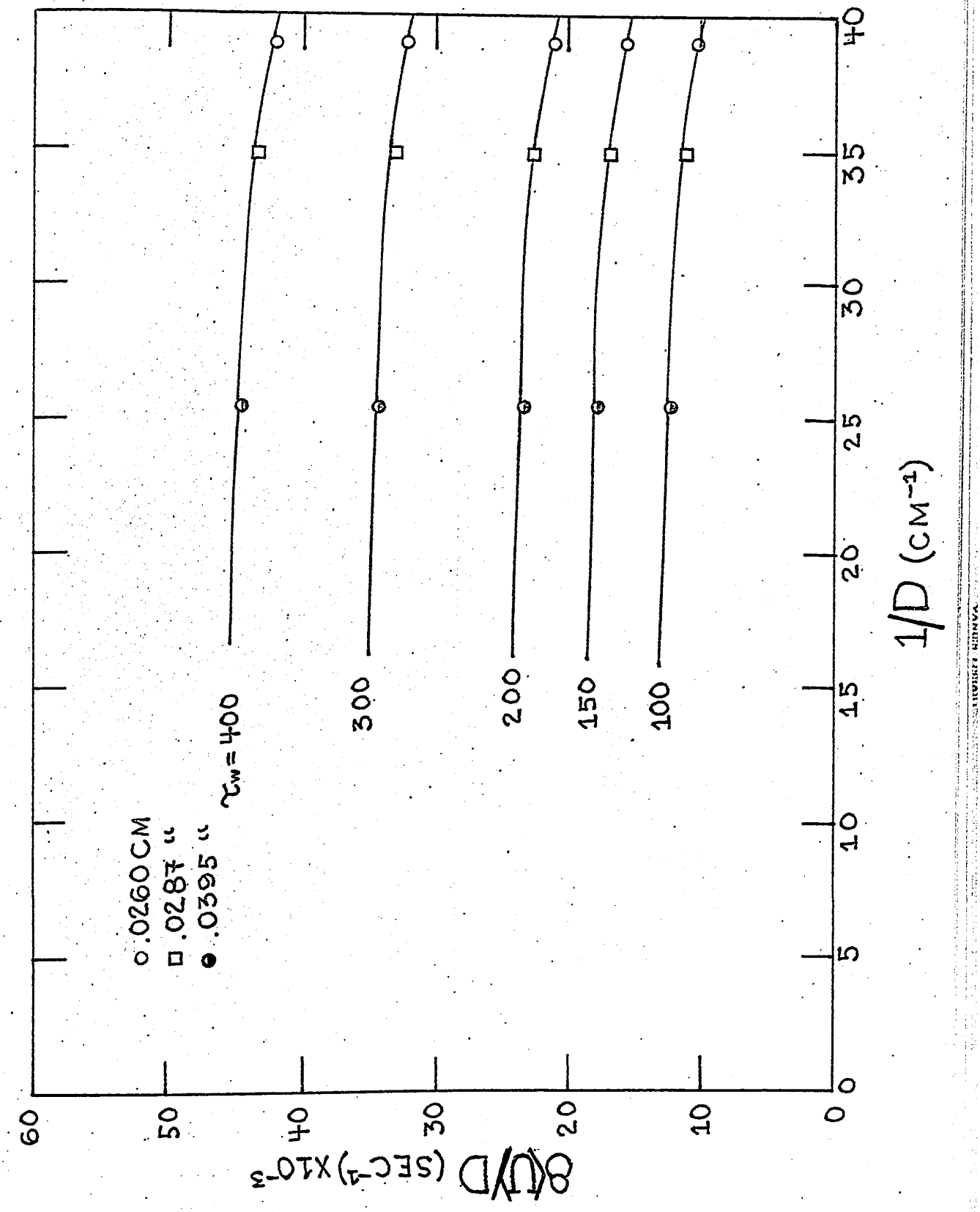


Fig. A-3 8 ⟨U⟩/D vs. 1/D Plot for a 20 ppm Polyox WSR-301 Solution

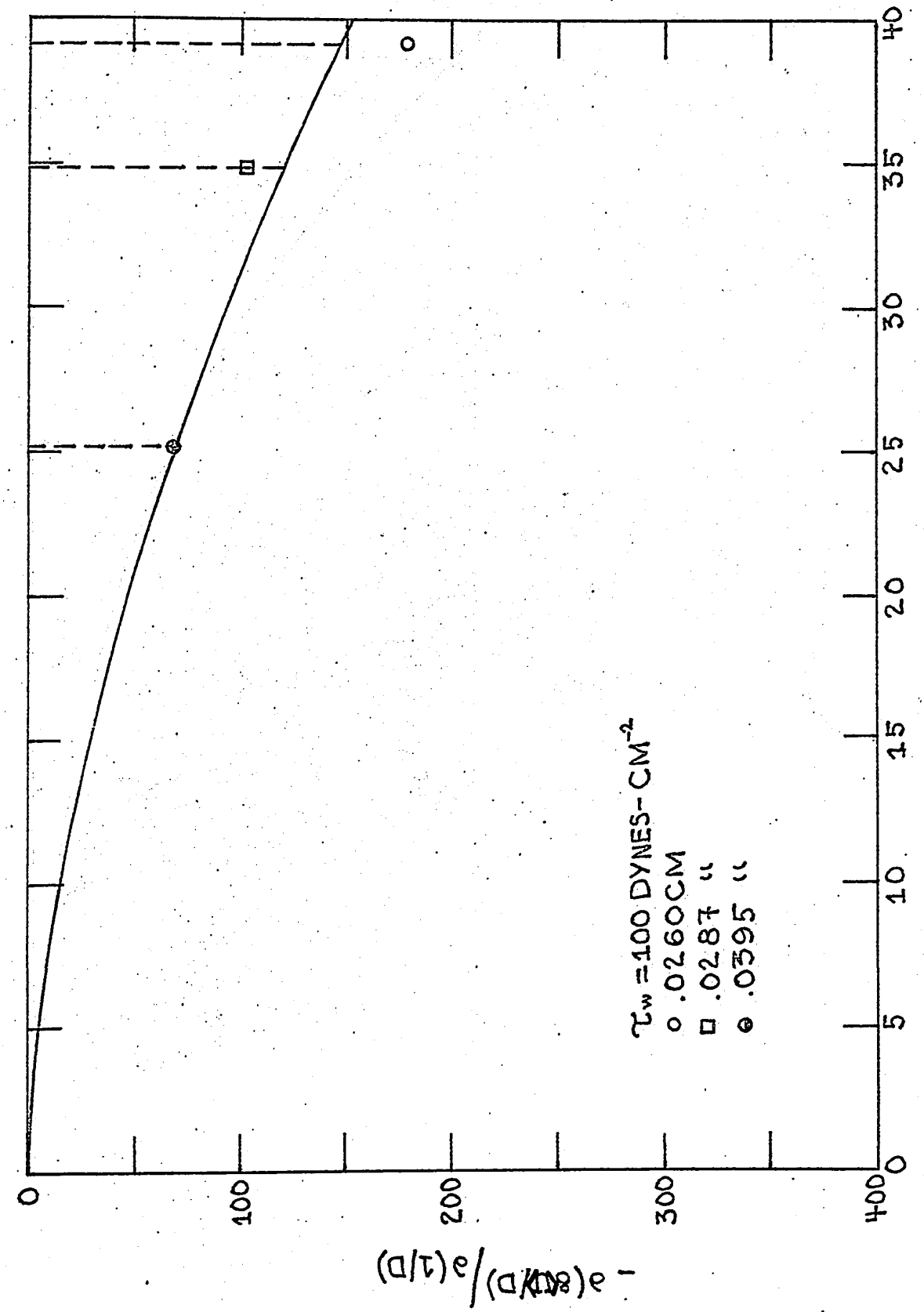


Fig. A-4 $\partial [8 \langle U \rangle / D] / \partial [1/D]$ vs. 1/D Plot for a 20 ppm Polyox WSR-301 Solution with Parameter $\tau_w$ = 100 Dynes/cm$^2$

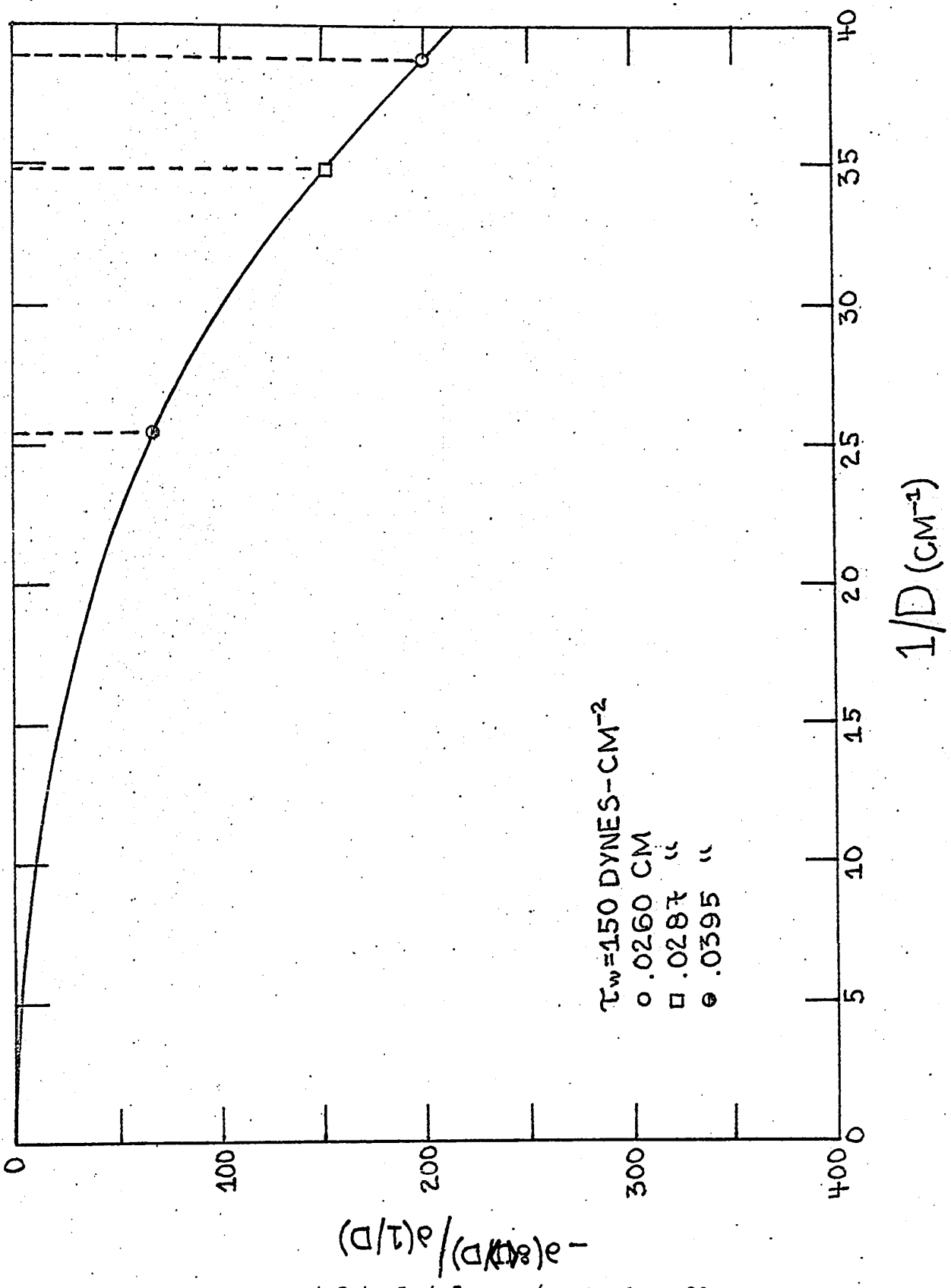


Fig. A-5 $\partial [8 \langle U \rangle / D] / \partial [1/D]$ vs. 1/D Plot for a 20 ppm Polyox WSR-301 Solution with Parameter $\tau_w$ = 150 Dynes/cm$^2$

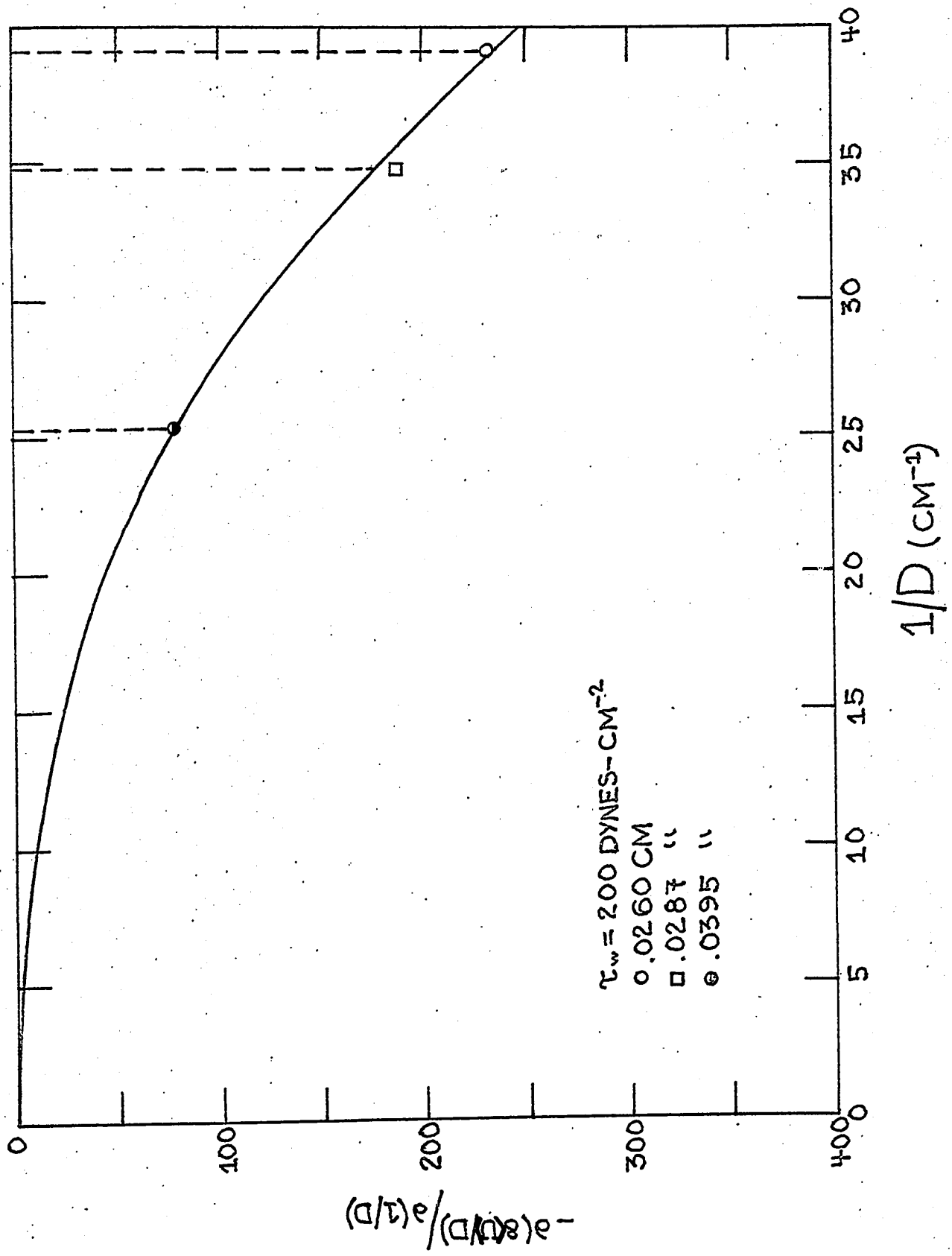


Fig. A-6 $\partial[8\langle U\rangle/D] / \partial[1/D]$ vs. 1/D Plot for a 20 ppm Polyox WSR-301 Solution with Parameter $\tau_w$ = 200 Dynes/cm$^2$

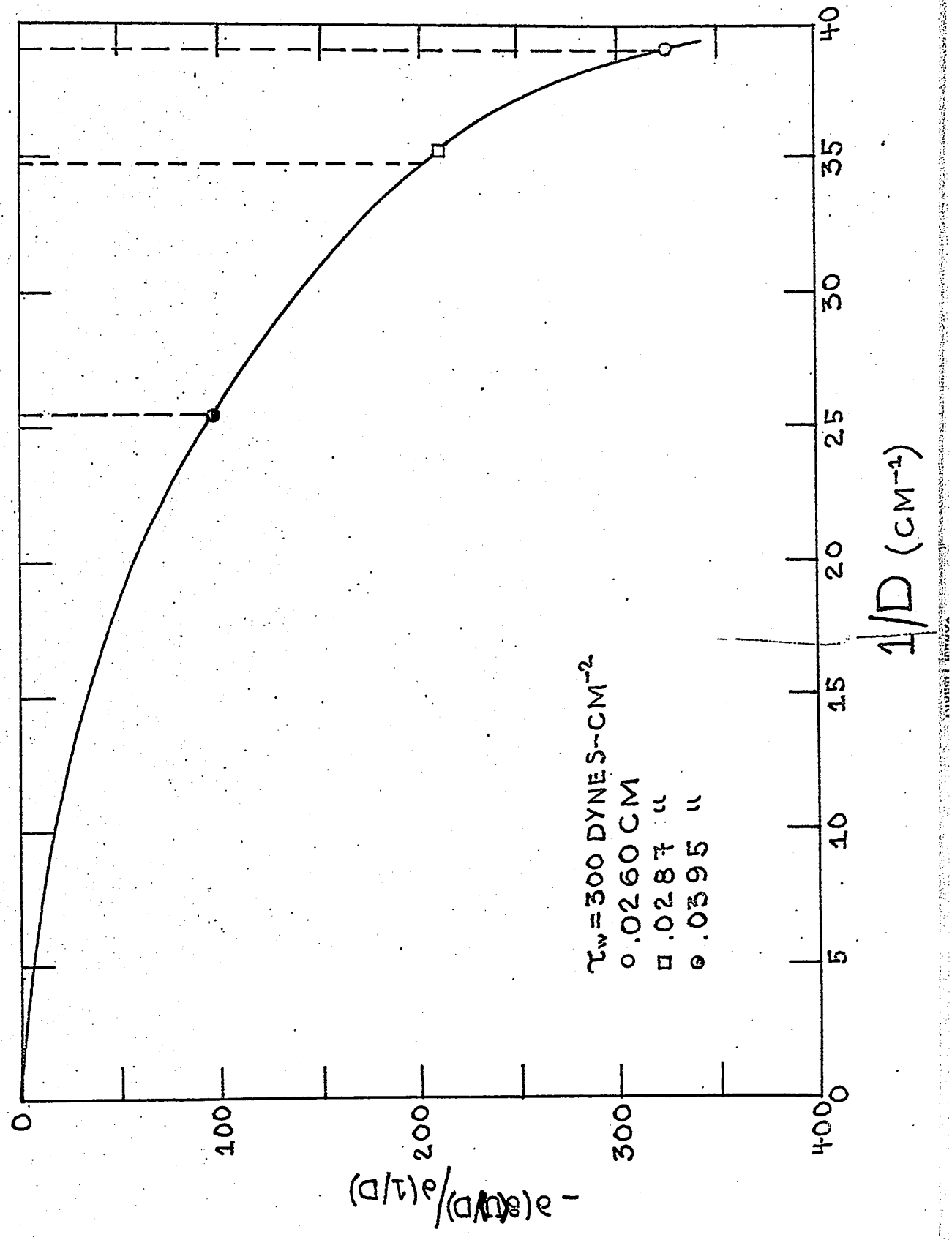


Fig. A-7 $\partial [8 \langle U \rangle / D] / \partial [1/D]$ vs. 1/D Plot for a 20 ppm Polyox WSR-301 Solution with Parameter $\tau_w$ = 300 Dynes/cm$^2$

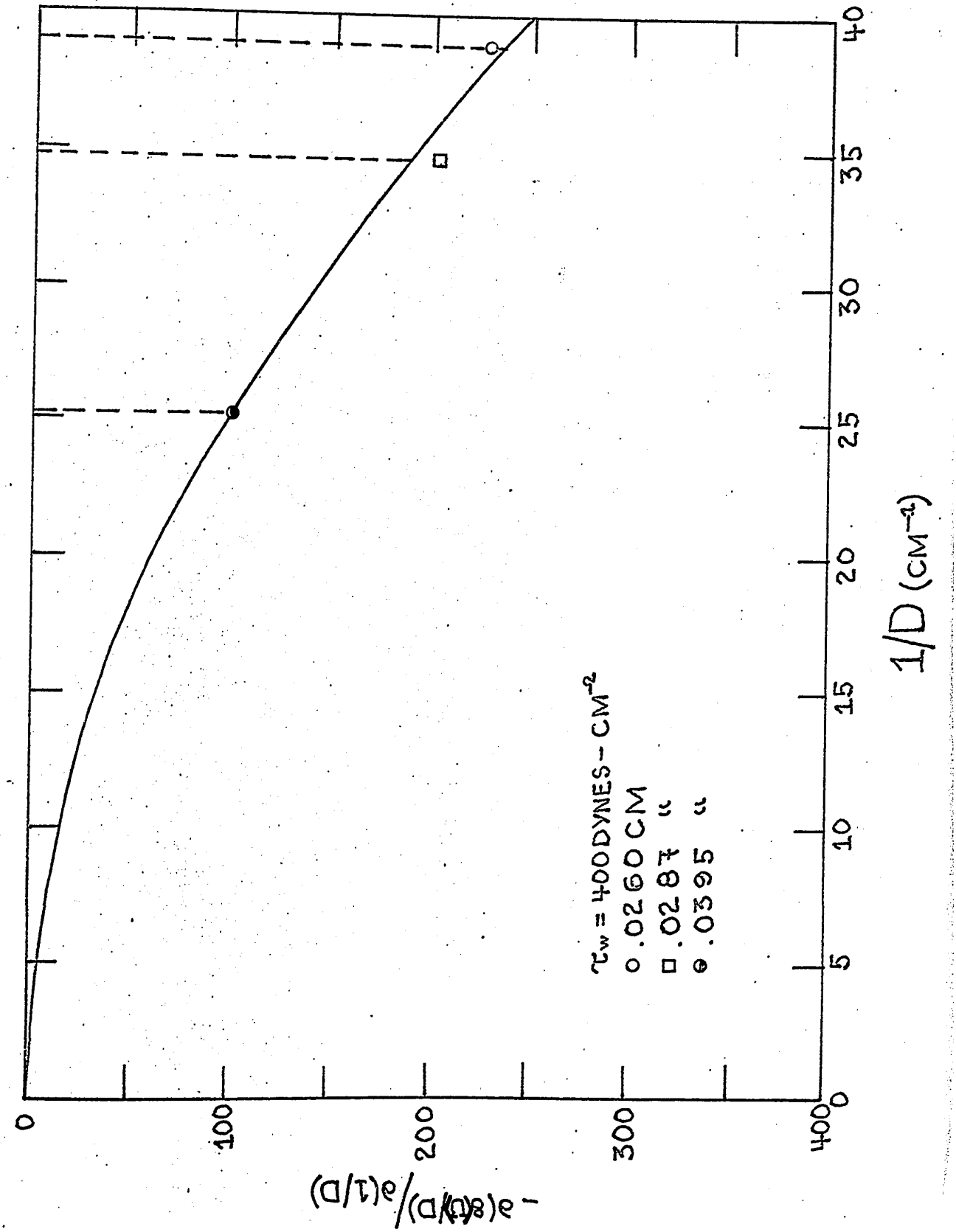


Fig. A-8 $\partial\,[8\,\langle U\rangle/D]\,/\,\partial\,[1/D]$ vs. 1/D Plot for a 20 ppm Polyox WSR-301 Solution with Parameter $\tau_w$ = 400 Dynes/cm$^2$

where

$$f(\tau_w) = \frac{1 + 3\eta'}{4\eta'} \left[\frac{8(\langle U\rangle - U_w)}{D}\right] \quad \text{..... (A-17)}$$

and

$$\eta' = \frac{d \ln \tau_w}{d \ln \left[\frac{8(\langle U\rangle - U_w)}{D}\right]} \quad \text{..... (A-18)}$$

so that, from the Uw calculated and tabulated in Table A-1, we can easily calculate δ. Those results are tabulated in Table A-2.

TABLE A-1

Calculations of $8(\langle U\rangle - U_w)/D$ for a 20 ppm Polyox WSR-301 Solution

| $\tau_w$ | 8 U/D | 1/D | Slope (-) | $-8U_w/D$ | $8(U - U_w)/D$ |
|---|---|---|---|---|---|
| 100 | 10,350 | 38.46 | 180 | 2,190.0 | 12,540.0 |
| | 10,900 | 34.84 | 100 | 1,704.8 | 12,604.8 |
| | 11,500 | 25.32 | 70 | 823.1 | 12,323.1 |
| 150 | 15,500 | 38.46 | 200 | 2,217.0 | 17,717.0 |
| | 16,200 | 34.84 | 150 | 1,594.4 | 17,794.4 |
| | 17,200 | 25.32 | 65 | 670.9 | 17,870.9 |
| 200 | 20,700 | 38.46 | 230 | 2,812.4 | 23,512.4 |
| | 21,500 | 34.84 | 190 | 2,066.7 | 23,566.7 |
| | 22,500 | 25.32 | 80 | 886.2 | 23,386.2 |
| 300 | 31,200 | 38.46 | 325 | 3,348.9 | 34,548.9 |
| | 32,200 | 34.84 | 210 | 2,418.6 | 34.618.6 |
| | 33,300 | 25.32 | 95 | 1,038.2 | 34.338.2 |

TABLE A-1 . . . continuation. . .

| $\tau_w$ | 8 U/D | 1/D | Slope (-) | - 8 $U_w$/D | 8 (U-$U_w$)/D |
|---|---|---|---|---|---|
| 400 | 42,000 | 38.46 | 225 | 3,254.1 | 45,254.1 |
| | 42,700 | 34.84 | 200 | 2,497.5 | 45,197.5 |
| | 44,100 | 25.32 | 100 | 1,164.7 | 45,264.7 |

| $\tau_w$ | 100 | 150 | 200 | 300 | 400 |
|---|---|---|---|---|---|
| Av. 8(U-$U_w$)/D | 12,489.3 | 17,794.1 | 23,488.4 | 34,501.9 | 45,238.8 |

TABLE A-2

Calculations of the Anomalous Layer Thickness

For a 20 ppm Polyox WSR-301 Solution

$\eta' = 1.047$ $\qquad \frac{1 + 3\eta'}{4\eta'} = .988$

| $\tau_w$ | 8 (U - $U_w$)/D | f ($\tau_w$) | D | - $U_w$ | $\delta$ |
|---|---|---|---|---|---|
| 100 | 12,250 | 12,103 | .0260 | 7.12 | $5.88 \times 10^{-4}$ |
| | | | .0287 | 6.12 | 5.06 |
| | | | .0395 | 4.06 | 3.35 |
| 150 | 17,800 | 17,586 | .0260 | 7.21 | $4.10 \times 10^{-4}$ |
| | | | .0287 | 5.72 | 3.25 |
| | | | .0395 | 3.31 | 1.88 |
| 200 | 23,500 | 23,318 | .0260 | 9.14 | $3.94 \times 10^{-4}$ |
| | | | .0287 | 7.41 | 3.19 |
| | | | .0395 | 4.38 | 1.89 |

TABLE A-2 ... continuation...

| $\tau_w$ | $8(U - U_w)/D$ | $f(\tau_w)$ | D | $-U_w$ | $\delta$ |
|---|---|---|---|---|---|
| 300 | 34,500 | 34,086 | .0260 | 10.88 | $3.19 \times 10^{-4}$ |
| | | | .0287 | 8.68 | 2.55 |
| | | | .0395 | 5.13 | 1.51 |
| 400 | 45,250 | 44,707 | .0260 | 10.58 | $2.37 \times 10^{-4}$ |
| | | | .0287 | 8.96 | 2.00 |
| | | | .0395 | 5.75 | 1.29 |

$$\delta = -U_w / f(\tau_w)$$

$$f(\tau_w) = \frac{1 + 3\eta'}{4\eta'} \left[\frac{8(U - U_w)}{D}\right]$$

$$\eta' = \frac{d \ln \tau_w}{d \ln \left[\frac{8(U - U_w)}{D}\right]}$$

# APPENDIX B

## TABULATION OF NON-NEWTONIAN FLOW BEHAVIOR INDEXES AND FLUID CONSISTENCY INDEXES FOR POLYOX WSR-301 SOLUTIONS

If we assume that the power-law model is applicable to the fluid flow situation encountered in our experiment[41], then we can relate the shear stress to the shear rate by the power-law relationship:

$$\tau_w = K^* \left[ \frac{8 (\langle U \rangle - U_w)}{D} \right]^{\eta'} \quad \ldots\ldots\ldots\ldots\ldots\ldots \text{(B-1)}$$

where

$$\eta' = \frac{d \ln \tau_w}{d \ln \left[ \frac{8 (\langle U \rangle - U_w)}{D} \right]} \quad \ldots\ldots\ldots\ldots\ldots\ldots \text{(B-2)}$$

is the flow behavior index and $K^*$ is the fluid consistency index.

Those values have been calculated for the different Polyox concentrations and are tabulated in Table B-1.

TABLE B-1

Non-Newtonian Fluid Characteristics

| Conc. (WPPM) | $\eta'$ (dimensionless) | $K^*$ ($gm\text{-}cm^{-1}\text{-}sec^{2-\eta'}$ |
|---|---|---|
| 20 | 1.047 | .0082 |
| 25 | 1.054 | .0084 |
| 30 | 1.032 | .0084 |
| 35 | 1.029 | .0088 |
| 40 | 1.042 | .0088 |

# APPENDIX C

## EXPERIMENTAL DATA AND RESULTS FOR THE FLOW OF POLYOX WSR-301 SOLUTIONS THROUGH CAPILLARY TUBES

TABLE C-1

Capillary Tubes Indentification

| Cap. No. | I. D. (cm) |
|---|---|
| 26 | .0260 |
| 24 | .0287 |
| 22 | .0395 |

TABLE C-2

Shear Stress - Shear Rate Data For a 20 ppm Polyox WSR-301 Solution at 25°C

| Cap. No. | $\tau_w$ (Dynes-cm$^{-2}$) | 8 ⟨U⟩/D (sec$^{-1}$) |
|---|---|---|
| 26 | 118.46 | 12,148.04 |
| | 155.05 | 16,042.30 |
| | 179.97 | 18,915.59 |
| | 204.89 | 21,393.37 |
| | 223.24 | 23,298.37 |
| | 241.56 | 25,145.31 |
| | 277.45 | 28,945.02 |
| 24 | 121.28 | 13,221.50 |
| | 162.56 | 17,521.41 |
| | 204.61 | 22,122.96 |
| | 239.78 | 25,782.40 |
| | 277.01 | 29,169.90 |
| | 309.09 | 33,172.19 |
| | 355.54 | 38,009.91 |
| 22 | 104.28 | 11,972.63 |
| | 155.65 | 17,835.79 |
| | 202.05 | 22,976.40 |
| | 239.74 | 27,217.73 |
| | 268.68 | 30,239.40 |
| | 307.08 | 34,134.77 |
| | 387.25 | 42,747.69 |

TABLE C-3

Shear Stress - Shear Rate Data For a 25 ppm Polyox WSR-301 Solution at 25°C

| Cap. No. | $\tau_w$ (Dynes-cm$^{-2}$) | 8 $\langle U \rangle / D$ (sec$^{-1}$) |
|---|---|---|
| 26 | 121.73 | 12,060.52 |
| | 153.30 | 15,547.06 |
| | 177.12 | 18,031.33 |
| | 207.78 | 21,290.28 |
| | 230.34 | 23,668.65 |
| | 255.19 | 26,060.44 |
| | 283.45 | 28,763.33 |
| 24 | 165.27 | 17,720.26 |
| | 199.46 | 21,177.19 |
| | 230.49 | 24,515.00 |
| | 255.69 | 27,165.83 |
| | 286.53 | 30,392.04 |
| | 214.20 | 33,268.06 |
| | 352.01 | 37,139.23 |
| 22 | 131.46 | 14,843.03 |
| | 165.54 | 18,749.93 |
| | 207.98 | 23,571.23 |
| | 236.06 | 26,552.88 |
| | 272.56 | 30,413.08 |
| | 322.02 | 35,478.94 |
| | 388.69 | 42,299.83 |

TABLE C-4

Shear Stress - Shear Rate Data For a 30 ppm Polyox WSR-301 Solution at 25°C

| Cap. No. | $\tau_w$ (Dynes-cm$^{-2}$) | 8 $\langle U \rangle$/D (sec$^{-1}$) |
|---|---|---|
| 26 | 126.96 | 12,463.81 |
| | 151.96 | 15,189.14 |
| | 173.46 | 17,495.10 |
| | 199.55 | 20,197.91 |
| | 227.11 | 23,053.16 |
| | 258.45 | 26,225.00 |
| | 287.90 | 28,758.27 |
| 24 | 123.22 | 12,546.73 |
| | 151.39 | 15,486.74 |
| | 178.51 | 18,204.21 |
| | 206.08 | 21,002.02 |
| | 248.04 | 25,285.21 |
| | 299.07 | 30,477.10 |
| | 360.07 | 36,535.63 |
| 22 | 118.54 | 13,300.13 |
| | 152.25 | 17,053.95 |
| | 194.87 | 21,825.91 |
| | 226.79 | 25,328.02 |
| | 270.73 | 30,226.46 |
| | 325.24 | 35,528.08 |
| | 402.39 | 43,395.10 |

TABLE C-5

Shear Stress - Shear Rate Data For a 35 ppm Polyox WSR-301 Solution at 25°C

| Cap. No. | $\tau_w$ (Dynes-cm$^{-2}$) | 8 ⟨U⟩ / D (sec$^{-1}$) |
|---|---|---|
| 26 | 110.59 | 10,279.28 |
| | 127.57 | 12,010.96 |
| | 149.50 | 14,475.71 |
| | 174.52 | 16,986.69 |
| | 211.38 | 20,626.84 |
| | 242.43 | 23,675.54 |
| | 280.65 | 27,448.71 |
| 24 | 122.63 | 12,739.02 |
| | 146.69 | 15,241.00 |
| | 176.95 | 18,295.40 |
| | 214.39 | 22,040.29 |
| | 254.74 | 26,201.96 |
| | 294.20 | 32,259.75 |
| | 386.96 | 39,680.41 |
| 22 | 107.23 | 11,894.07 |
| | 130.58 | 14,532.86 |
| | 163.04 | 18,176.63 |
| | 202.40 | 22,352.65 |
| | 245.03 | 27,126.75 |
| | 295.32 | 32,482.00 |
| | 349.77 | 38,179.16 |

TABLE C-6

Shear Stress - Shear Rate Data For a 40 ppm Polyox WSR-301 Solution at 25°C

| Cap. No. | $\tau_w$ (Dynes-cm$^{-2}$) | 8 $\langle U \rangle$/D (sec$^{-1}$) |
|---|---|---|
| 26 | 115.22 | 11,156.84 |
| | 130.23 | 12,861.61 |
| | 149.50 | 14,773.45 |
| | 171.41 | 16,949.75 |
| | 193.67 | 19,233.66 |
| | 237.76 | 23,517.88 |
| | 288.60 | 28,585.40 |
| 24 | 134.17 | 13,896.93 |
| | 156.10 | 16,192.48 |
| | 179.05 | 18,445.95 |
| | 211.26 | 21,757.13 |
| | 238.18 | 24,515.08 |
| | 302.72 | 30,787.04 |
| | 376.50 | 38,065.31 |
| 22 | 129.57 | 14,364.97 |
| | 154.96 | 17,160.28 |
| | 187.76 | 20,916.17 |
| | 212.31 | 23,406.13 |
| | 243.46 | 27,013.14 |
| | 275.98 | 30,730.16 |
| | 355.53 | 38,859.08 |

TABLE C-7

Effective Velocity of Slip and Anomalous Layer Thickness
For a 20 ppm Polyox WSR-301 Solution at 25°C

| Cap. No. | $\tau_w$ (Dynes-cm$^{-2}$) | $-U_w$ (cm-sec$^{-1}$) | $\delta$ (cm) |
|---|---|---|---|
| 26 | 100 | 7.12 | .000588 |
| 24 | | 6.12 | 506 |
| 22 | | 4.06 | 335 |
| 26 | 150 | 7.21 | 410 |
| 24 | | 5.72 | 325 |
| 22 | | 3.31 | 188 |
| 26 | 200 | 9.14 | 394 |
| 24 | | 7.41 | 319 |
| 22 | | 4.38 | 189 |
| 26 | 300 | 10.88 | 319 |
| 24 | | 8.68 | 255 |
| 22 | | 5.13 | 151 |
| 26 | 400 | 10.58 | 237 |
| 24 | | 8.96 | 200 |
| 22 | | 5.75 | 129 |

TABLE C-8

Effective Velocity of Slip and Anomalous Layer Thickness

For a 25 ppm Polyox WSR-301 Solution at 25°C

| Cap. No. | $\tau_w$ (Dynes-cm$^{-2}$) | $-U_w$ (cm-sec$^{-1}$) | $\delta$ (cm) |
|---|---|---|---|
| 26 | 100 | 5.81 | .000491 |
| 24 | | 4.16 | 351 |
| 22 | | 1.88 | 159 |
| 26 | 150 | 7.42 | 430 |
| 24 | | 5.51 | 319 |
| 22 | | 2.50 | 145 |
| 26 | 200 | 9.22 | 406 |
| 24 | | 6.74 | 297 |
| 22 | | 3.13 | 138 |
| 26 | 300 | 9.34 | 282 |
| 24 | | 5.87 | 177 |
| 22 | | 1.69 | 051 |
| 26 | 400 | 7.85 | 181 |
| 24 | | 6.11 | 141 |
| 22 | | 2.06 | 047 |

TABLE C-9

Effective Velocity of Slip and Anomalous Layer Thickness

For a 30 ppm Polyox WSR-301 Solution at 25°C

| Cap. No. | $\tau_w$ (Dynes-cm$^{-2}$) | $-U_w$ (cm-sec$^{-1}$) | $\delta$ (cm) |
|---|---|---|---|
| 26 | 100 | 6.15 | .000525 |
| 24 | | 4.89 | 418 |
| 22 | | 2.31 | 197 |
| 26 | 150 | 8.42 | 488 |
| 24 | | 7.45 | 432 |
| 22 | | 4.94 | 286 |
| 26 | 200 | 11.39 | 499 |
| 24 | | 9.66 | 423 |
| 22 | | 6.25 | 274 |
| 26 | 300 | 9.72 | 288 |
| 24 | | 7.02 | 208 |
| 22 | | 3.13 | 093 |
| 26 | 400 | 11.32 | 254 |
| 24 | | 7.24 | 162 |
| 22 | | 2.63 | 059 |

TABLE C-10

Effective Velocity of Slip and Anomalous Layer Thickness For a 35 ppm Polyox WSR-301 Solution at 25°C

| Cap. No. | $\tau_w$ (Dynes-cm$^{-2}$) | $-U_w$ (cm-sec$^{-1}$) | $\delta$ (cm) |
|---|---|---|---|
| 26 | 100 | 7.37 | .000645 |
| 24 | | 3.91 | 342 |
| 22 | | 0.87 | 076 |
| 26 | 150 | 7.98 | 478 |
| 24 | | 4.53 | 272 |
| 22 | | 1.25 | 075 |
| 26 | 200 | 8.61 | 390 |
| 24 | | 5.81 | 263 |
| 22 | | 2.50 | 113 |
| 26 | 300 | 8.21 | 251 |
| 24 | | 5.81 | 177 |
| 22 | | 2.50 | 076 |
| 26 | 400 | 9.90 | 228 |
| 24 | | 6.71 | 155 |
| 22 | | 2.75 | 063 |

TABLE C-11

Effective Velocity of Slip and Anomalous Layer Thickness
For a 40 ppm Polyox WSR-301 Solution at 25°C

| Cap. No. | $\tau_w$ (Dynes-cm$^{-2}$) | $-U_w$ (cm-sec$^{-1}$) | $\delta$ (cm) |
|---|---|---|---|
| 26 | 100 | 4.56 | .000401 |
| 24 | | 3.45 | 303 |
| 22 | | 1.88 | 165 |
| 26 | 150 | 6.18 | 367 |
| 24 | | 4.80 | 285 |
| 22 | | 2.38 | 141 |
| 26 | 200 | 7.95 | 358 |
| 24 | | 6.03 | 272 |
| 22 | | 3.13 | 141 |
| 26 | 300 | 9.59 | 294 |
| 24 | | 7.15 | 220 |
| 22 | | 3.50 | 107 |
| 26 | 400 | 11.14 | 260 |
| 24 | | 6.87 | 160 |
| 22 | | 2.88 | 067 |

# APPENDIX D

## ERROR EVALUATIONS AND DISCUSSION

## Error Evaluations and Discussion

Because of the simple design of the experimental set-up, the causes of errors have been reduced to a minimum. Nevertheless, those we could not eliminate were accounted for, as much as possible, and are listed below, in order of increasing importance:

1. the circulating water temperature
2. the liquid head above the capillary tubes
3. the mercury manometer readings
4. the tube length effect.

The temperature of the circulating water varied very little, mainly because the thermoregulator kept it within 0.01°C of the set temperature but also because the ambient temperature itself was also around 25°C.

On the other hand, the liquid head above the tubes did vary during a sample collection, but the effect of such a continuous drop was very small because of the large surface of the reservoir (161 $cm^2$) compared to the size of the capillary tube and to the volume of solution collected (5 to 20 cc). The overall error caused by the liquid head drops on the shear stress values was calculated for each sample and was found to vary between .07 to 1.02% with the average value being around 0.2%.

In reading the liquid head above the tubes however, the divisions were indicated in millimeters, thereby giving us a maximum reading accuracy of $\pm$ 0.05 cm. or approximately $\pm$ 0.5% on those readings.

The mercury manometer had divisions of 0.1 cm therefore allowing a maximum reading accuracy of $\pm$ 0.05 cm. Over the range of pressures used in our experiment, this means a percentage error varying between $\pm$ 0.1% and $\pm$ 0.5% of each pressure reading.

The last major cause of error, namely the effect of the length of the tubes is more complex and harder to evaluate in our case. An L/D ratio of at least 200 is required in order to obtain a fully developed, steady velocity profile at the tube exit. And even though our L/D ratios were all at least twice that value, the velocity profile was still not fully developed over the entrance length of the tube. Now, in all our calculations, we assume that $\tau_w$ is constant over the whole length of the tubes while in fact, its value starts from zero at the entrance of the tube, increases to a steady value over approximately the first 200 L/D value and then, stays constant for the rest of the length of the tube.

A program was initiated this summer to evaluate the importance of this effect but the results did not prove very satisfactory and we are therefore left to rely on the results as they are.

# APPENDIX E

## SUPPLEMENTARY DATA

Shear Stress - Shear Rate Data For a 20 ppm Polyox WSR-301 Solution at 25°C

| Cap. No. (Diam. in cm.) | $\tau_w$ (Dynes-cm$^{-2}$) | 8 $\langle U \rangle$/D (sec$^{-1}$) |
|---|---|---|
| 20 (.0578) | 105.00 | 12,446.35 |
| | 168.60 | 19,485.91 |
| | 212.11 | 24,122.16 |
| | 256.11 | 28,573.37 |
| | 308.46 | 33,454.60 |
| | 363.93 | 38,983.35 |
| | 438.63 | 45,597.73 |
| 18 (.0799) | 116.65 | 13,028.96 |
| | 154.38 | 16,793.59 |
| | 208.96 | 21,992.60 |
| | 255.74 | 26,219.63 |
| | 304.43 | 30,570.94 |
| | 341.20 | 33,428.65 |
| | 369.33 | 36,309.27 |

Shear Stress - Shear Rate Data For a 25 ppm Polyox WSR-301 Solution at 25°C

| Cap. No. (Diam. in cm.) | $\tau_w$ (Dynes - cm$^{-2}$) | 8 ⟨U⟩/D (sec$^{-1}$) |
|---|---|---|
| 20 (.0578) | 104.92 | 12,287.66 |
| | 171.02 | 19,439.93 |
| | 224.86 | 25,296.12 |
| | 277.53 | 30,446.39 |
| | 332.63 | 35,988.27 |
| | 388.37 | 41,621.87 |
| | 462.59 | 47,783.91 |
| 18 (.0799) | 86.44 | 9,730.48 |
| | 152.62 | 16,480.63 |
| | 196.48 | 20,723.46 |
| | 235.72 | 24,280.29 |
| | 276.85 | 28,090.35 |
| | 322.27 | 31,494.46 |
| | 356.02 | 34,819.31 |

Shear Stress - Shear Rate Data For a 30 ppm Polyox WSR-301 Solution at 25°C

| Cap. No. (Diam. in cm.) | $\tau_w$ (Dynes-cm$^{-2}$) | 8 ⟨U⟩/D (sec$^{-1}$) |
|---|---|---|
| 20 (.0578) | 122.99 | 14,226.96 |
| | 157.99 | 18,342.42 |
| | 209.30 | 23,555.15 |
| | 264.93 | 29,315.65 |
| | 309.46 | 33,581.12 |
| | 346.13 | 37,299.73 |
| | 406.83 | 41,720.54 |
| 18 (.0799) | 117.48 | 13,092.06 |
| | 146.54 | 16,000.44 |
| | 182.25 | 19,403.60 |
| | 224.35 | 23,206.63 |
| | 262.31 | 26,779.63 |
| | 294.60 | 29,433.40 |
| | 330.89 | 32,682.94 |

Shear Stress - Shear Rate Data For a 35 ppm Polyox WSR-301 Solution at 25°C

| Cap. No. (Diam. in cm.) | $\tau_w$ (Dynes - $cm^{-2}$) | 8 ⟨U⟩/D ($sec^{-1}$) |
|---|---|---|
| 20 (.0578) | 134.82 | 15,530.50 |
| | 167.13 | 18,943.32 |
| | 202.08 | 22,868.40 |
| | 245.52 | 27,415.27 |
| | 305.75 | 33,053.33 |
| | 357.19 | 37,727.25 |
| | 411.80 | 43,227.90 |
| 18 (.0799) | 112.66 | 12,213.59 |
| | 149.65 | 16,194.97 |
| | 180.68 | 19,302.36 |
| | 211.72 | 22,034.50 |
| | 263.40 | 26,614.73 |
| | 313.23 | 30,621.23 |
| | 359.13 | 34,194.44 |

Shear Stress - Shear Rate Data For a 40 ppm Polyox WSR-301 Solution at 25°C

| Cap. No. (Diam. in cm.) | $\tau_w$ (Dynes - $cm^{-2}$) | 8 ⟨U⟩/D ($sec^{-1}$) |
|---|---|---|
| 20 (.0578) | 143.02 | 16,256.64 |
| | 174.24 | 19,787.45 |
| | 208.21 | 23,628.66 |
| | 264.04 | 28,945.71 |
| | 316.24 | 34,375.98 |
| | 394.03 | 41,659.06 |
| | 486.93 | 51,219.02 |
| 18 (.0799) | 122.03 | 13,303.61 |
| | 157.50 | 16,682.27 |
| | 185.76 | 19,663.85 |
| | 221.16 | 22,896.15 |
| | 274.92 | 27,832.94 |
| | 343.78 | 32,757.56 |
| | 406.44 | 38,293.98 |